The bacterial defense system MADS interacts with CRISPR-Cas to limit phage infection and escape

Alice Maestri, Benoit Pons, Elizabeth Pursey, Charlotte Chong, Sylvain Gandon, Rafael Custodio, Anna Olina, Aleksei Agapov, Matthew A.W. Chisnall, Anita Grasso, et al.

Article

Cell Host & Microbe

The bacterial defense system MADS interacts with CRISPR-Cas to limit phage infection and escape

Graphical abstract

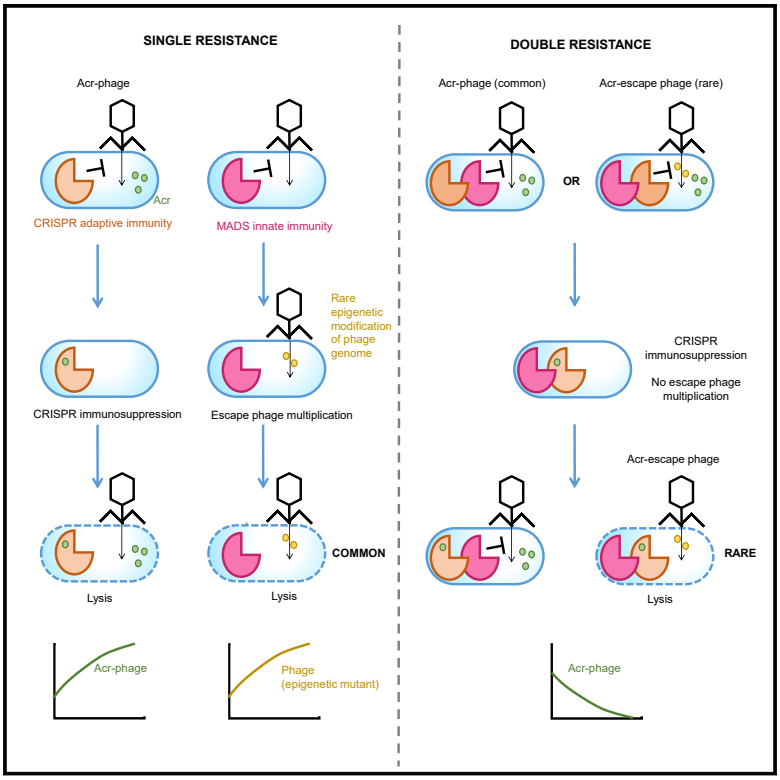

Highlights

- Methylation-associated defense system (MADS) is a complex bacterial innate immune system
- MADS function relies on nuclease, ATPase, kinase, and methyltransferase domains
- MADS is distributed across gram-positive and gram-negative bacteria
- MADS and CRISPR-Cas interplay provides strong and durable protection against phages

Authors

Alice Maestri, Benoit J. Pons, Elizabeth Pursey, ..., Stineke van Houte, Anne Chevallereau, Edze R. Westra

Correspondence

anne.chevallereau@cnrs.fr (A.C.), E.R.westra@exeter.ac.uk (E.R.W.)

In brief

The coevolution between bacteria and mobile genetic elements has resulted in a large diversity of defense systems. Maestri et al. describe an innate immune system, MADS (methylation-associated defense system), that interacts with CRISPR-Cas in its native host to provide strong and long-term protection against phages.

Maestri et al., 2024, Cell Host & Microbe *32*, 1412–1426
August 14, 2024
https://doi.org/10.1016/j.chom.2024.07.005

CellPress

CellPress
OPEN ACCESS

Cell Host & Microbe

Article

The bacterial defense system MADS interacts with CRISPR-Cas to limit phage infection and escape

Alice Maestri,[1] Benoit J. Pons,[1,7] Elizabeth Pursey,[1,9,7] Charlotte E. Chong,[2,5,7] Sylvain Gandon,[3] Rafael Custodio,[1] Anna Olina,[1] Aleksei Agapov,[1] Matthew A.W. Chisnall,[1] Anita Grasso,[1,10] Steve Paterson,[2] Mark D. Szczelkun,[4] Kate S. Baker,[2,5] Stineke van Houte,[1] Anne Chevallereau,[6,8,11,*] and Edze R. Westra[1,8,*]

[1]Environment and Sustainability Institute, Biosciences, University of Exeter, Penryn TR10 9FE, UK
[2]Institute of Infection, Veterinary and Ecological Sciences, University of Liverpool, Liverpool L69 7ZB, UK
[3]CEFE, CNRS, Université de Montpellier, EPHE, IRD, Montpellier 34293, France
[4]DNA-Protein Interactions Unit, School of Biochemistry, University of Bristol, Bristol BS8 1TD, UK
[5]Department of Genetics, University of Cambridge, Downing Place, Cambridge CB2 3EH, UK
[6]Université Paris Cité, CNRS, INSERM, Institut Cochin, Paris 75014, France
[7]These authors contributed equally
[8]These authors contributed equally
[9]Present address: Department of Experimental Medicine, University of Lund, Lund 221 84, Sweden
[10]Present address: Department of Clinical Microbiology, Trinity College Dublin 24, Ireland
[11]Lead contact
*Correspondence: anne.chevallereau@cnrs.fr (A.C.), E.R.westra@exeter.ac.uk (E.R.W.)
https://doi.org/10.1016/j.chom.2024.07.005

SUMMARY

The constant arms race between bacteria and their parasites has resulted in a large diversity of bacterial defenses, with many bacteria carrying multiple systems. Here, we report the discovery of a phylogenetically widespread defense system, coined methylation-associated defense system (MADS), which is distributed across gram-positive and gram-negative bacteria. MADS interacts with a CRISPR-Cas system in its native host to provide robust and durable resistance against phages. While phages can acquire epigenetic-mediated resistance against MADS, co-existence of MADS and a CRISPR-Cas system limits escape emergence. MADS comprises eight genes with predicted nuclease, ATPase, kinase, and methyltransferase domains, most of which are essential for either self/non-self discrimination, DNA restriction, or both. The complex genetic architecture of MADS and MADS-like systems, relative to other prokaryotic defenses, points toward highly elaborate mechanisms of sensing infections, defense activation, and/or interference.

INTRODUCTION

Mobile genetic elements (MGEs) are important drivers of the ecology and evolution of their bacterial hosts,[1] and in response to MGE infections, bacteria have evolved a plenitude of defense systems.[2] Dozens of previously unknown defenses were discovered in recent years,[3–9] often aided by their clustering in defense islands.[10,11] Defense systems can be characterized by a relatively simple genetic architecture, comprising one-gene systems, such as nuclease-helicase immunity (Nhi), that cleave the genome of invading MGEs,[12] or can have a more complex makeup with multiple genes acting in concert, such as CRISPR-Cas (clustered regularly interspaced short palindromic repeats—CRISPR-associated genes), relying on immune memory based interference.[13] Several defense systems frequently coexist in the same genome,[10,11,14,15] a factor that can prevent the emergence of spontaneous phage mutants that overcome host resistance. For example, the co-existence of restriction-modification (RM) and CRISPR-Cas leads to a reduction in the frequency of spontaneous phage mutants that "escape" both defenses, as well as a higher rate of CRISPR immunity acquisition.[16–18] In response to prokaryotic immunity, many phages have evolved sophisticated counter-defense mechanisms that specifically block bacterial defense systems, such as anti-RM,[19] anti-CRISPR (Acr),[20] and the more recently identified anti-CBASS,[21,22] anti-Pycsar,[22] and anti-TIR-STING[23] proteins. Recent studies showed that Acr proteins are often imperfect and that phages coding for Acr (i.e., Acr-phages) need to cooperate to overcome CRISPR immunity of the bacteria they infect.[24,25] We set out to study how general these observations are by studying the infection dynamics of phage DMS3, which encodes an Acr that blocks the type I-E CRISPR-Cas immune system of *Pseudomonas aeruginosa* SMC4386. This resulted in the serendipitous discovery of a complex innate immune system of bacteria that interacts with CRISPR-Cas in its native host.

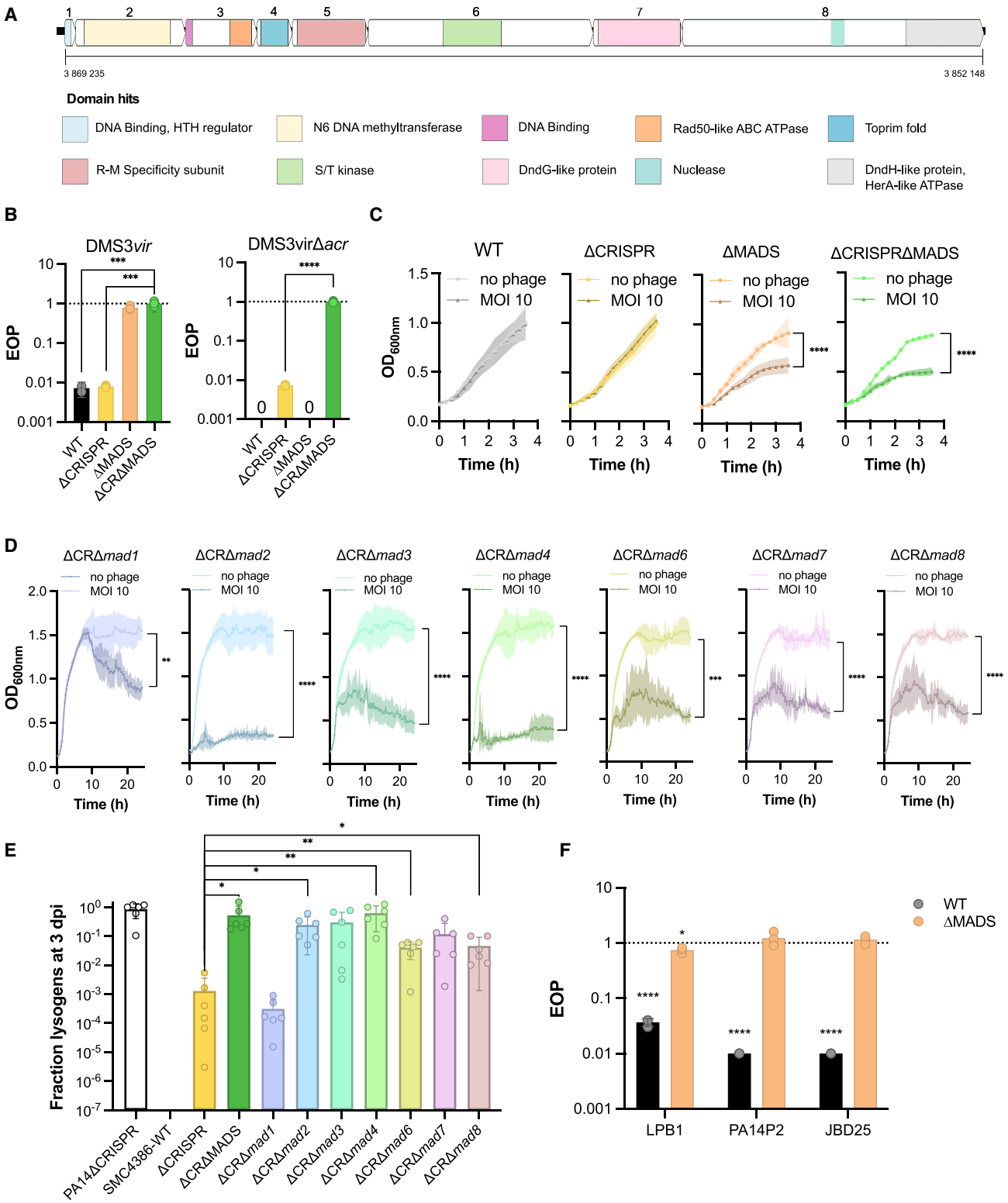

Figure 1. MADS protects bacteria against phage infections

(A) MADS is an 8-gene operon. Numbers in the top arrows correspond to gene numbering (*mad1-mad8*). Colors in bottom arrows indicate domain hits predicted with HHpred and AlphaFold2 analyses (see Data S1); the scale indicates the position of the *mad* operon on the SMC4386 genome assembled as single chromosome (in bp).

(legend continued on next page)

RESULTS

Discovery of the defense system coined MADS

The type I-E CRISPR-Cas immune system of *P. aeruginosa* SMC4386 carries a spacer that perfectly matches the genome of phage DMS3, which carries the gene *acrIE3* that blocks the CRISPR-Cas system.[26] Previous studies with *P. aeruginosa* PA14 showed that some Acrs are imperfect and that Acr-phages can amplify only if their density exceeds a critical threshold.[24,25] However, while phage DMS3*vir*, a c-repressor mutant locked in the lytic cycle, successfully adsorbed to *P. aeruginosa* SMC4386 (Figure S1A), it was unable to amplify on the SMC4386 wild-type (WT) nor on the ΔCRISPR strain, even at the highest starting phage inoculum (Figures S1B and S1C). Moreover, infection experiments with the temperate phage DMS3-Gm, a mutant of phage DMS3 that carries a gentamycin resistance gene,[24] revealed that no lysogens were formed on the SMC4386 strain (Figure S1D), despite AcrIE3 efficiently blocking the type I-E CRISPR-Cas immune system of SMC4386 (Figure S1E).

Based on these observations, we hypothesized that *P. aeruginosa* SMC4386 may carry additional defense systems that limit DMS3 infectivity. To test this prediction, we generated transposon (Tn) mutant libraries of the WT and SMC4386ΔCRISPR strains, which we then infected with DMS3-Gm, resulting in lysogen formation (Figure S1F). Sanger sequencing revealed Tn insertions in *cas* genes and in a specific genomic region containing a predicted operon of 8 genes (Figure S1G). This 17-kb putative operon did not contain a known complete defense system based on PADLOC and DefenseFinder analyses[27,28] (Table S1) at the time of the discovery. However, PADLOC identified 3 genes in this operon as putative components of DNA modification systems: a kinase, a specificity subunit, and a methyltransferase (Table S1). Therefore, we hypothesized that this operon encodes a defense system, which we coined methylation-associated defense system (MADS) (Figure 1A). Interestingly, this operon contains predicted domains that are also found in other bacterial defense systems (Data S1), including: a small helix-turn-helix protein (MAD1) which may provide transcriptional regulation or sequester phage proteins; a site-specific adenine methyltransferase (MAD2 and MAD5) related to type I and type II RM enzymes that epigenetically tags host DNA as "self"; an OLD family related ATP-dependent system (MAD3 and MAD4) which could act as a supplementary nuclease effector; a serine/threonine kinase domain-containing protein (MAD6) that may play similar roles as in Bacteriophage exclusion (BREX) family systems in signaling responses to infection or in system regulation; and two subunits (MAD7 and MAD8) that are related to the subunits of the ATP-dependent nuclease effector of phosphorothioate (PT)-dependent restriction systems which target unmodified DNA (Data S1).

To test whether MADS mediates phage resistance, we knocked out ~22 kb of the genome encompassing this operon (referred to as ΔMADS). Plaque assays with phage DMS3*vir* showed a 100-fold increase in the efficiency of plaquing (EOP) on ΔMADS compared with the WT strain (Figure 1B). Likewise, the EOP of DMS3*vir*Δ*acr* lacking the *acrIE3* gene increased by approximately 100-fold on a double mutant ΔCRISPRΔMADS compared with ΔCRISPR (Figure 1B). Moreover, when MADS was absent, bacteria displayed normal growth in the absence of phage DMS3*vir* but reduced growth in its presence (Figure 1C), whereas bacteria carrying MADS grew equally well in the presence and absence of phage at a multiplicity of infection (MOI) of 10 (Figure 1C). Furthermore, infection assays with the ΔCRISPRΔMADS strain revealed phage amplification regardless of the initial phage inoculum (Figure S2A), whereas infection of the ΔMADS strain required a threshold density to support phage amplification (Figure S2B). Such threshold is explained by Acr-phages-induced immunosuppression of the host (Figure S2C), in accordance with previous observations made with phages carrying *acrIF* genes and bacteria with type IF CRISPR-Cas immunity.[24,25]

Having established that MADS provides resistance against phage DMS3, we next wanted to test the role of each gene in mediating this phenotype (*mad1-8*, Figures 1D and 1E). We therefore generated knockout mutants of each individual *mad* gene in the ΔCRISPR background and measured how this impacted phage resistance. Interestingly, despite repeated attempts, we were unable to delete *mad5*, unless *mad2* or *mad3* were also deleted, suggesting that deletion of *mad5* alone is lethal. Infection experiments showed that individual gene deletions of *mad2-4* and *mad6-8* all resulted in reduced bacterial growth in the presence of phage DMS3*vir*, whereas deletion of *mad1* had limited effect (Figure 1D). Moreover, deletion of either the full system or each of the individual *mad* genes resulted in a 30- to 400-fold increase in phage DMS3 lysogens formation in mutant backgrounds relative to the ΔCRISPR strain, except for *mad1* (Figure 1E).

To verify whether our single-gene-deletions may have caused any polar effect that could influence the phenotype observed, we cloned each *mad* gene in a multi-copy plasmid (see STAR Methods) and checked if knockouts could be rescued via spot test of phage DMS3*vir* (Figure S1H).

Of note, despite numerous endeavors, we were unable to clone *mad8* unless without promoter, presumably because its putative nuclease activity is toxic for the cell.

Overall, complementations tend to restore the original phenotypes (i.e., the ΔCRISPR background), with some knockouts being fully rescued, such as *Δmad1* and *Δmad6*, and others being partially rescued (Figure S1H). Interestingly, while phage-impaired bacterial growth of *Δmad6* and *Δmad7* mutants in

(B) Efficiency of plating (EOP) of phage DMS3*vir* or DMS3*vir*Δ*acr* on strains SMC4386-WT, ΔCRISPR, ΔMADS, and ΔCRISPRΔMADS.
(C and D) Bacterial growth curves of WT and mutant strains in absence or presence of phage DMS3*vir* (with multiplicity of infection, MOI, of 10). Single *mad* gene deletions are all in a ΔCRISPR background (indicated as ΔCRΔ*madX*, with X the gene number).
(E) Fraction of the bacterial population carrying the DMS3 prophage (lysogens) at 3 days post-infection (dpi) in WT and mutant SMC4386 backgrounds, as indicated. ΔCR is an abbreviation for ΔCRISPR.
(F) EOP of phages LBP1, JBD25, and PA14P2 on SMC4386-WT and the isogenic ΔMADS strain. For each panel, values for individual biological replicates are shown (3 replicates in B and F, 4 replicates in C and D, and 6 replicates in E) as well as mean values. Errors bars (B, E, and F) and shaded areas (C and D) show 95% confidence intervals (c.i.). Details of the statistical tests are provided in Table S2.

CellPress
OPEN ACCESS

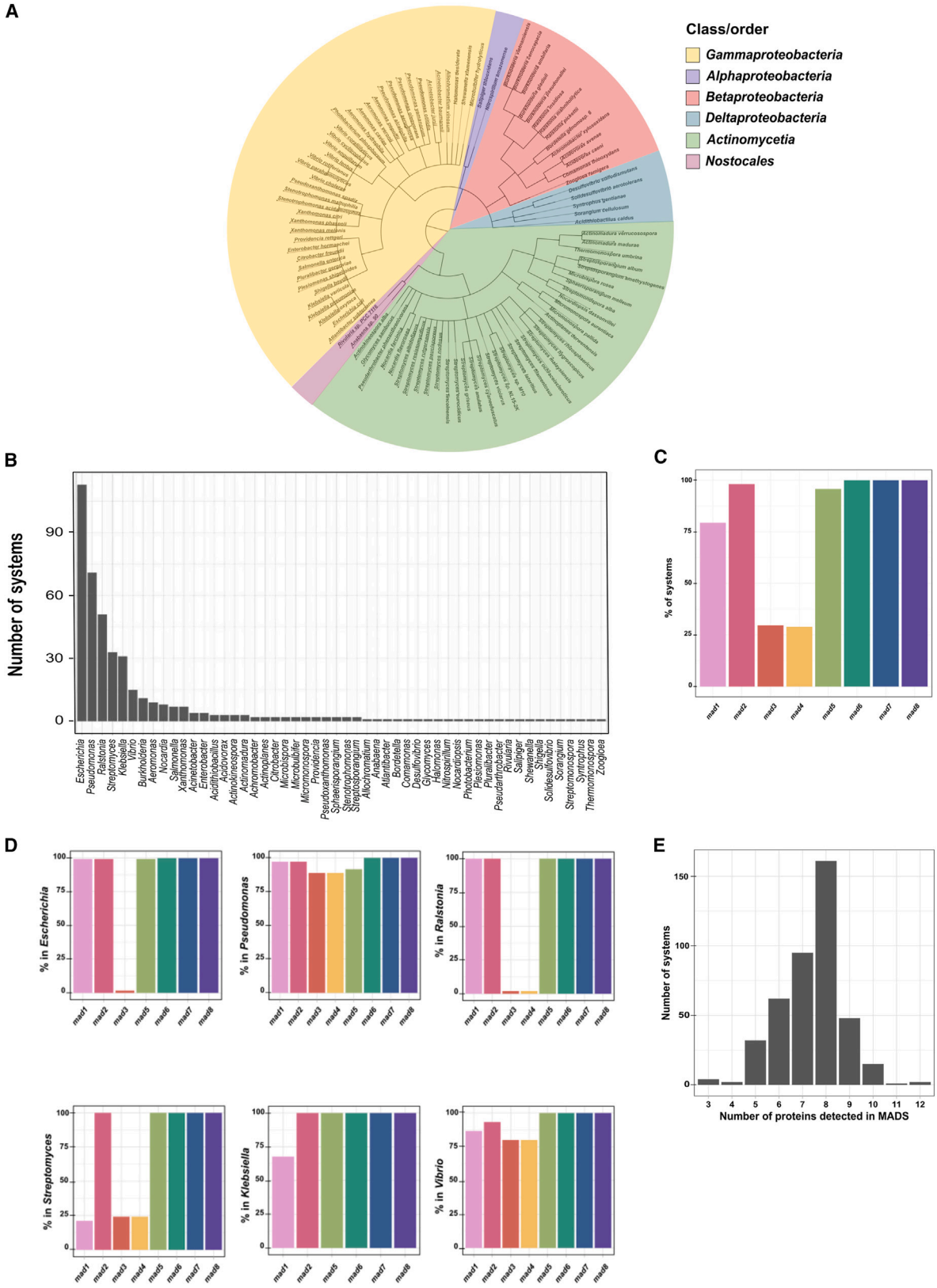

(legend on next page)

liquid growth media (Figure 1D), deletion of *mad1*, *mad6*, and *mad7* resulted in a 10- to 100-fold reduction in EOP compared with the parental ΔCRISPR strain (Figure S1H). The apparent discrepancy between bacterial survival in liquid culture and plaque formation on solid media could be due to differences in the physiological state of bacteria, regulation of the system, or activation of abortive infection (abi) phenotypes that impacts plaque formation while not promoting cell growth. In addition, deletion of *mad* genes with putative regulatory roles (e.g., *mad1* and *mad6*) could be associated with increased resistance levels (Data S1). To understand the range of protection offered by MADS, we carried out spot test assays with diverse phages, including temperate phages LPB1 (*Casadabanvirus*) and JBD25 (*Caudoviricetes*), and PA14P2 (*Beetrevirus*), carrying two phage transposition genes but which lifestyle is predicted to be virulent based on BACPHLIP[29] analyses (86% probability, Rosanna Wright, personal communication). We observed a similar increase (>10-fold) in the EOP of all phages in the ΔMADS strain relative to the SMC4386-WT (Figure 1F). Based on these data, we conclude that MADS encodes a defense system that is active against at least 4 different DNA phages, with genes *mad2-4* and *mad6-8* seemingly being essential for phage resistance.

Distant bacterial classes carry MADS

To determine how widespread and conserved MADS is, we built a MacSyFinder model[30] and searched through all bacterial and archaeal genomes in the RefSeq database (downloaded in January 2022). We identified 422 MADS in 100 different species belonging to *Alpha, Beta, Gamma*, and *Deltaproteobacteria*, *Actinobacteria*, and *Nostocales* (Figure 2A). The *mad1-8* operon was most commonly found in the genera *Escherichia* (n = 113), *Pseudomonas* (n = 71), *Ralstonia* (n = 51), *Streptomyces* (n = 33), *Klebsiella* (n = 31), and *Vibrio* (n = 15) (Figure 2B), presumably reflecting their overrepresentation in the database. This analysis also revealed variation in the gene content of MADS operons (Figures 2C–2E), which could be due to genetic divergence, alternative MADS subtypes, or the existence of degenerate systems. Detection of MADS was next incorporated into PADLOC, and a subsequent search on a recent RefSeq database (v209, kindly shared with us by Dr. Simon Jackson) found MADS in 0.3% of the genomes (706/233,092) (Table S3), with all of the hits being in *Bacteria* (706/706). The frequency of MADS in the genera where it is most commonly found is 0.5% (111/ 21,143) in *Escherichia*, 1.2% (77/6,243) in *Pseudomonas*, 21% (51/244) in *Ralstonia*, 4.4% (60/1,349) in Streptomyces, and 0.5% (35/6,501) in *Klebsiella* (Table S3). Overall, while small dissimilarities in MADS counts could be attributable to the different amounts of genomes present in each database and to the detection method itself, our analyses revealed that MADS is a widespread but rare defense system. Additionally, we analyzed the co-occurrence between MADS and CRISPR-Cas in the whole RefSeq database and in the MADS-enriched genera and found that MADS and any CRISPR-Cas system co-occur in 0.1% of the genomes in RefSeq database and in less than 3% of the genomes from the MADS-enriched genera (Table S3).

Manual inspection of 66 *P. aeruginosa* genomes containing the complete MADS operon showed that, in 77% of the cases (51/66), the operon was located within a recently described defense island.[31] We identified this island of 9.5–2,402.9 kb (average = 64.3 kb) in 97% of the complete *P. aeruginosa* genomes available at the time of the search, September 2022 (Figure 3A; Table S4), and confirmed that it is significantly enriched for defense systems compared with the remainder of the genome (median of 0.1 systems/kb vs. 0.003 systems/kb, Wilcoxon's signed rank test, $p < 0.05$) (Figure 3B; Table S4). Analysis of the defense systems within this island revealed 46 different known defense systems, as well as potentially novel or incomplete defense systems (Figure 3C; Data S1), including an operon related to MADS that we coined "MADS-like": this is an 11-gene system (numbered *madl1* to *madl11*), which was found in 10/444 islands (Figures 3D–3E; Data S1). Interestingly, both MADS and MADS-like are predicted to encode an N6 methyladenosine MTase (Figure 3D; Data S1), which suggests that self/non-self discrimination relies on DNA methylation.[32]

CRISPR-dependent emergence of epigenetic phage mutants that escape MADS

To experimentally test whether MADS uses epigenetic modification for self/non-self discrimination, we co-cultured phage DMS3*vir* and SMC4386ΔCRISPR and monitored whether phages gained the capability to overcome MADS. When the ΔCRISPR strain was infected with phage DMS3*vir*, we noticed phage amplification at 2 dpi in some of the replicates (Figure 4A). Phages from these populations were isolated, and their infectivity was measured on different SMC4386 mutant backgrounds. This test revealed that such phages had become insensitive to MADS (Figure 4B). To test whether they acquired epigenetic modifications, we next amplified these phages successively on PA14ΔCRISPR (which lacks MADS) and SMC8346-WT. We predicted that phages would lose their insensitivity to MADS following amplification on the PA14 background. Consistent with this hypothesis, phages that replicated on PA14ΔCRISPR had a decreased infectivity when they were next passaged on the SMC4386-WT strain (Figure 4C, PA14 → SMC), whereas this pattern was not observed in the control treatments (Figure 4C, SMC → PA14, SMC → SMC, or PA14 → PA14).

Interestingly, escape phages with epigenetic mutations to overcome MADS did not arise during infection of the WT strain, suggesting the presence of a strong interaction between CRISPR-Cas and MADS that prevents the evolutionary emergence of such phage escape variants (Figure 4A).

Figure 2. Distribution and configuration of MADS loci in bacterial genomes

(A) Minimal tree showing the taxonomic distribution of MADS across bacterial phylogeny.

(B) The number of MADS detected in each genus in descending order.

(C and D) Percentage of systems containing each *mad* gene (*mad1-8*) within the detected MADS across all RefSeq genomes (n = 422) (C) and percentage of systems containing each *mad* gene (*mad1-8*) for each genus where 15 or more systems were identified (D).

(E) The number of systems detected according to total number of proteins (>8 is possible where there are multiple hits to the same protein HMM, hidden Markov model).

CellPress
OPEN ACCESS

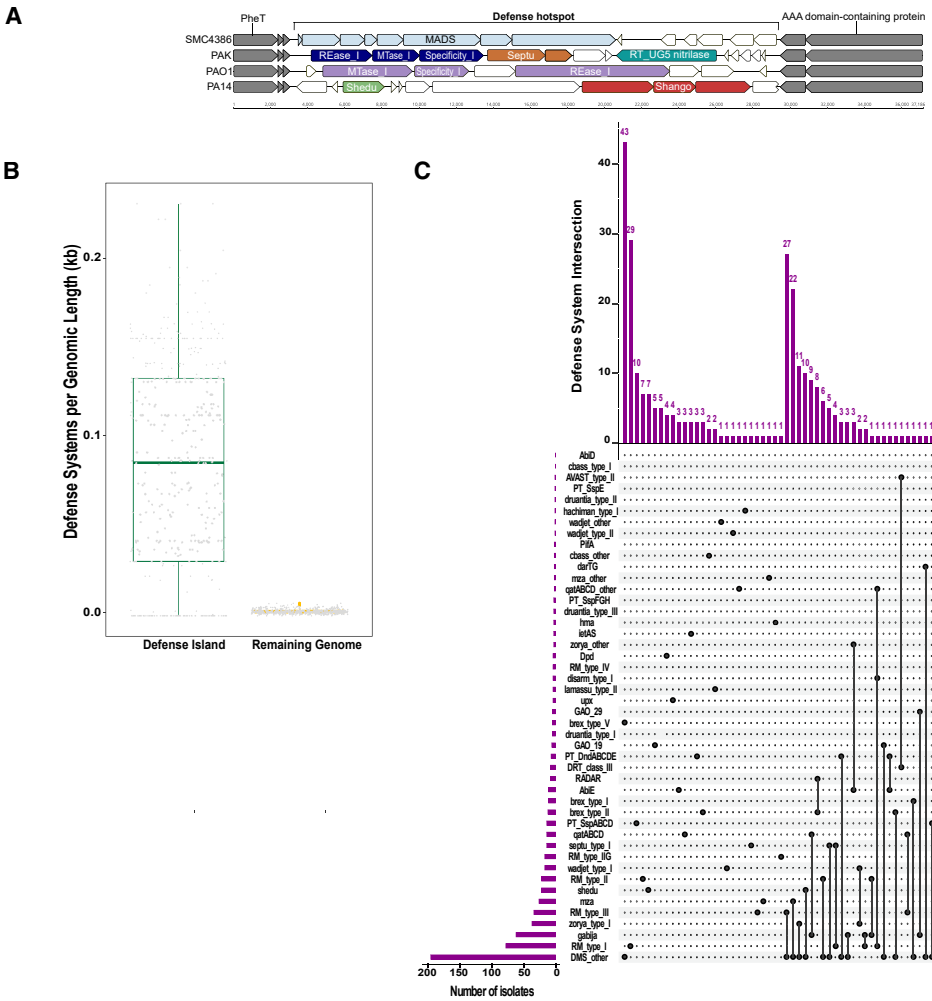

(legend on next page)

We suspected that this might be due to imperfect blocking of the type I-E CRISPR-Cas system by the phage-encoded *acrIE3* gene, when the strain carries an additional defense system. We explored this hypothesis first using a mathematical model (Figure S2D and STAR Methods), which suggests that the threshold density for Acr-phages amplification increases when bacteria carry another defense system in addition to CRISPR-Cas (Figure S2E), as this additional defense may prevent the exploitation of CRISPR-immunosuppressed cells by Acr-phages. Moreover, the model predicts that the likelihood of emergence of MADS escape phages depends on the presence or absence of CRISPR-Cas immunity, with escape phages emerging only at higher densities when the levels of CRISPR immunity increase (Figure S2F).

To test these model predictions, we carried out infection experiments of the WT and ΔCRISPR strains using different phage initial MOIs and tracked the frequencies of MADS escape phages. Infection of the ΔCRISPR strain revealed that from 2 dpi, phage densities often started to increase due to the emergence of MADS escape phages (Figure 4D, red circles). These escape phages were identified in 20 out of 42 (47%) independent experiments spanning different initial phage MOIs, from 10^4 plaque forming unit (PFU)/mL to 10^9 PFU/mL (corresponding to MOI of 10^{-3} to 10^2). By contrast, on WT bacteria, escape phages emerged in 12% of the replicates (5 out of 42), and only when the initial phage MOIs were very high (Figure 4E, red circles). Moreover, increase of phage population density was only observed in 1 out of these 6 replicates (Figure 4E).

Next, we sought to investigate the contribution of escape phages to the total phage population amplification during mixed infections of hosts carrying neither (CRISPR or MADS) single or double resistance (Figure S2G). As expected, we observed phage amplification above 10^5 PFU/mL, the starting inoculum of WT phage DMS3*vir*, only during infections of the strains lacking MADS (i.e., ΔMADS and ΔCRISPRΔMADS), regardless of the initial density of methylated phages (Figure S2G), while phage amplification occurred only at the highest initial inocula of escape phages during infections of the ΔCRISPR strain, and no amplification on the WT strain was observed (Figure S2G). A control assay with DMS3*vir* escape phages alone showed that these phages amplify on strains carrying CRISPR (i.e., ΔMADS and WT) only if their density exceeds a minimal threshold concentration of 10 PFU/mL (Figures S2B and S2H), consistent with our theoretical predictions of the effect of MADS defense on Acr-phages amplification on bacteria with CRISPR immunity (Figure S2E). This shows that while the *acrIE3* encoded by phage DMS3*vir* is strong, rare epigenetic mutants that overcome MADS are less likely to amplify when bacteria carry CRISPR immunity compared with strains that only have MADS (Figure S2H). Finally, consistent with our previous observations, a control assay with WT phages DMS3*vir* (i.e., non-escape) alone showed that phage amplification only occurs during infections of strain lacking MADS (Figure S2I).

Based on these data, we conclude that MADS and CRISPR-Cas efficaciously interact in the SMC4386 strain by limiting the emergence and spread of MADS escape mutants.

Identification of the MADS target sequence

Next, we wanted to obtain a better understanding of the mechanism of MADS defense. To identify the nature and site of epigenetic modification generated by MADS, we carried out PacBio sequencing of the escape phages and the ancestral DMS3*vir* phage. Sequencing results revealed that the motif 5′-TCAGNNNNTCC-3′ has m6A modifications at positions 3 and 9 on the positive and negative strands, respectively, in the escape phages but not in the ancestral phage genome (Figure 5A). The phage has 7 such motifs, all of which were methylated in the escape phages. Moreover, PacBio sequencing of the bacterial DNA revealed that the same motifs were methylated on the bacterial chromosome in the SMC4386-WT and ΔCRISPR strains, whereas these sites were not methylated in the ΔCRISPRΔMADS nor in the ΔCRISPRΔ*mad2* strain, which encodes the predicted methyltransferase. The combination of phenotypic and sequencing data therefore supports the hypothesis that MADS uses a methylation-based self/non-self discrimination mechanism. To further corroborate the hypothesis that MADS provides resistance against MGEs with an unmethylated 5′-TCAGNNNNTCC-3′ sequence but not against MGEs with a methylated sequence, we measured the transformation efficiency of methylated and unmethylated plasmids carrying the target sequence relative to plasmids without this sequence. Consistent with our hypothesis, a methylated plasmid carrying

Figure 3. Known and potential novel defense systems

(A) Composition of the genomic island in strains SMC4386, PAK, PAO1, and PA14. Conserved genes forming the boundaries of the island are indicated in gray. Colored arrows indicate genes forming indicated defense systems.

(B) Number of defense systems per genomic length (kb) in the defense island compared with the remaining genome. Boxplots display the interquartile range, median, and maximum defense systems per genomic length (kb) in the defense island and the remaining genome. Each gray dot represents density values for each isolate.

(C) UpSet plot indicating the co-occurrence of defense systems (identified with PADLOC) in genomic island. Genotypic defense system profiles are shown in the combination matrix in the center panel, where each column represents a unique genotypic presence/absence profile. Each black dot represents the presence of a defense system. The vertical bar plot above the matrix displays the number of isolates with a genotypic profile. The horizontal bar plot on the left of the matrix illustrates the proportion of isolates that contain each defense system.

(D) Comparison of the MADS and MADS-like putative defense systems. Predicted protein domains (HHpred) are indicated with colored boxes. Protein domains that are common between MADS and MADS-like are indicated in bold characters. More refined domain identification for MADS as presented in Figure 1A was based on AlphaFold2 structure predictions (Figures S4–S7).

(E) Ten defense islands that carry the MADS-like system (orange) have nearly identical genetic architecture. Blue, red, green, and yellow arrows highlight type IV RM, Yqaj recombinase, Tiamat, and site-specific integrase, respectively. Gray arrows mark the boundaries of the defense islands. The top panel indicates an additional defense island carrying the MADS-like system identified in Johnson et al.[31] Boxes show groups of genes that are present in the top island but not in the bottom island, and vice versa. Light yellow arrows in the top box highlight genes encoding conjugation system and plasmid partitioning proteins. Details of the statistical tests are provided in Table S2.

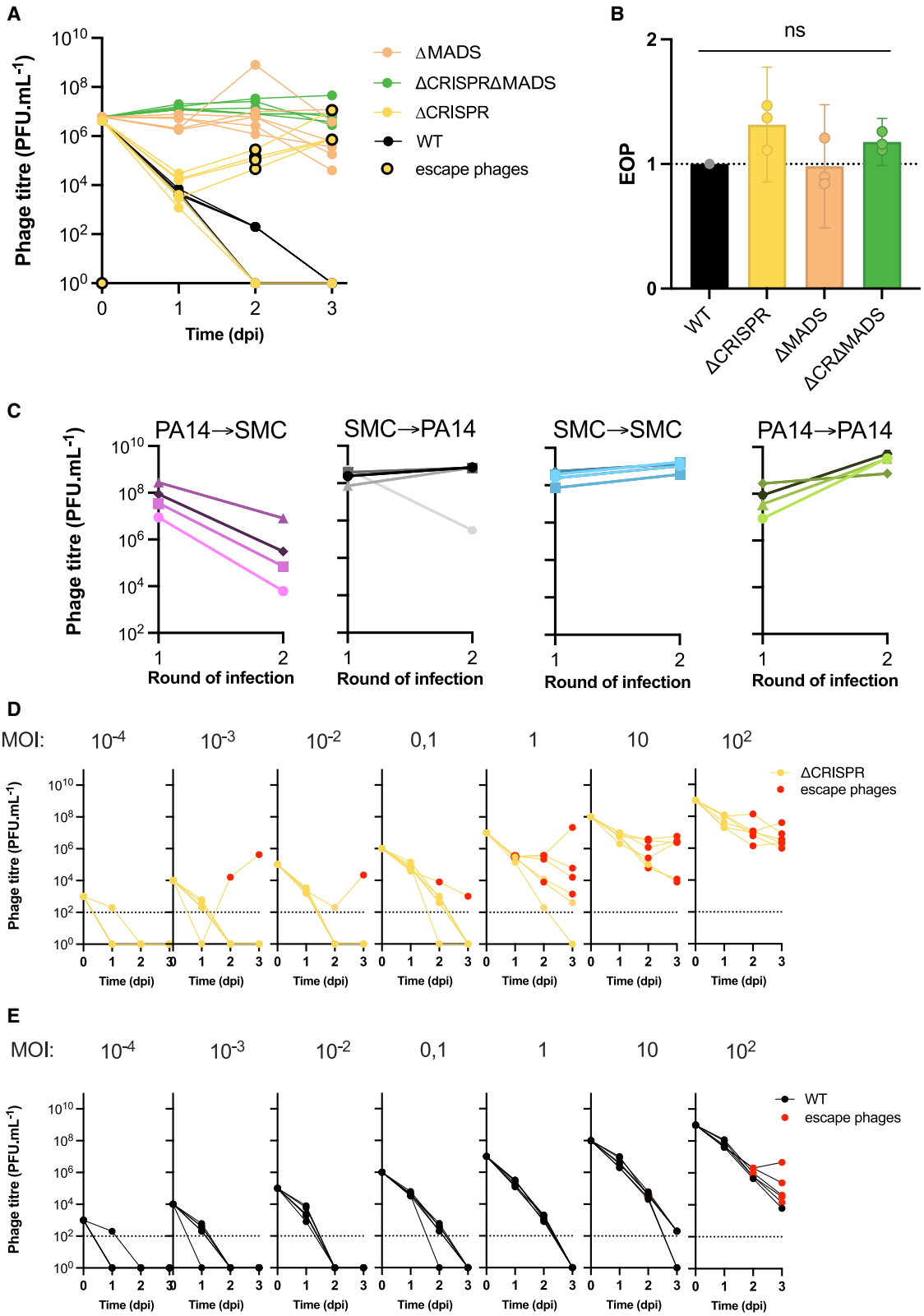

Figure 4. Phages escape MADS through epigenetic modification

(A) Titer of phage DMS3*vir* over 3 dpi (MOI 0.1) of strains SMC8386-WT, ΔCRISPR, ΔMADS, or ΔCRISPRΔMADS. Yellow circles with black outline indicate replicates from which DMS3*vir* escape phages were isolated. Data are shown for 6 individual biological replicates.

(legend continued on next page)

a 5′-TCAGCGCGTCC-3′ sequence had a 100-fold increased relative transformation efficiency (RTE) compared with the non-methylated plasmid when recipient cells carried MADS, while no differences could be observed when strains lacked MADS (Figure 5B). Hence, recognition of the unmethylated target sequence by MADS is required for mediating resistance against MGE infections.

MADS genes responsible for methylation and restriction activities

Having determined the target sequence of the MADS system, we then explored which MADS genes are required for methylation of the 5′-TCAGNNNNTCC-3′ sequence. We amplified a target plasmid carrying this sequence, or a non-target plasmid control, in the different SMC4386 single *mad* gene knockout strains. These plasmids were then used to measure RTE in ΔCRISPR and ΔCRISPRΔMADS strains (Figure 5C). Plasmids produced in the ΔCRISPRΔ*mad1*, Δ*mad3*, and Δ*mad6*-8 strains had a RTE close to 1 in both the ΔCRISPR and ΔCRISPRΔMADS strains (Figure 5C), meaning that those plasmids are efficiently methylated. However, the RTE of plasmids produced in the ΔCRISPRΔ*mad2*, Δ*mad5*Δ*mad2*, Δ*mad5*Δ*mad3* strains and in the ΔCRISPR ΔMADS control strain is around 10^{-2} when transformed into recipient cells with a functional MADS system. Hence, the genes *mad2* (methyltransferase) and *mad5* (specificity subunit) are essential for methylation. Interestingly, plasmids produced in the ΔCRISPRΔ*mad4* strain have an RTE around 10^{-1} in the ΔCRISPR strains, suggesting a partial methylation.

We then sought to validate our findings with an *in vitro* assay. We modified the targeted plasmid to incorporate an EcoRI site that overlaps with the MADS restriction site so that methylation of the MADS restriction site prevents cleavage by the EcoRI enzyme. This plasmid was amplified in each of the SMC4386 MADS mutants, as above, and digested with NheI (to linearize the plasmid) and EcoRI (to test for methylation). This confirmed that plasmids produced in the ΔCRISPRΔ*mad1*, Δ*mad3*, and Δ*mad6-8* strains were protected from EcoRI digestion, with the proportion of non-digested plasmid close to 100% (Figure 5D), indicating effective and complete methylation. Conversely, plasmids produced in the ΔCRISPRΔ*mad2*, Δ*mad5*Δ*mad2*, Δ*mad5*Δ*mad3* strains and in the ΔCRISPRΔMADS control strain were sensitive to EcoRI cleavage, and the proportion of non-digested plasmid was less than 1% (Figure 5D), which confirms that deletion of *mad2* and *mad5* abolishes methylation. This experiment also confirmed that deletion of *mad4* (encoding a predicted protein with DUF4276 domain) leads to incomplete protection, with a proportion of non-digested plasmid close to 40% (Figure 5D).

To investigate which of the MADS genes are responsible for the restriction activity, we calculated the RTE of non-methylated and methylated plasmids in each mutant (Figure 5E). As expected, the RTE of methylated plasmid was around 1 for all tested strains. The RTE of non-methylated plasmids was 10^{-2}–10^{-3} on the ΔCRISPR strain and around 1 on the ΔCRISPRΔMADS strain. On the ΔCRISPRΔ*mad3*, Δ*mad6-8*, Δ*mad5*Δ*mad2*, and Δ*mad5*Δ*mad3* strains, the RTE was also around 1, whereas the RTE on ΔCRISPRΔ*mad1*, Δ*mad2*, and Δ*mad4* mutants was significantly below 1 (Figure 5E). However, while *mad1*, *mad2*, and *mad4* are not essential for restriction activity, the RTE values for these mutants were higher than those of the ΔCRISPR strain, suggesting that deletion of these genes affects the efficacy of restriction activity.

Proposed mechanistic model for MADS activity

Finally, we used structural modeling to refine our functional predictions of the components of the MADS immune system (Data S1). This analysis revealed that a MAD2:MAD5 complex is highly likely to form the N6 methyladenosine MTase (Figure 6), with a close homology to $HsdS_1$:$HsdM_2$ MTase structures and bipartite DNA methylation sequences seen in type I and IIB RM systems. The diversity of recognition sequences recognized by type I enzymes is driven by recombination between *hsdS* genes that are akin to *mad5*,[33] and it is possible that MADS benefits from similar genetic exchanges. The deletion of *mad5* is toxic, which would be consistent with loss of self-protection by DNA modification. That *mad2* deletion is not toxic despite loss of DNA methylation may suggest that MAD2 acts as a hub for assembly of at least part of the restriction complex and/or a controlling signaling complex. Co-deletion of *mad2* and *mad5* thus prevents toxicity. Co-deletion of *mad3* and *mad5* also reduced toxicity, suggesting that it may also play a role in assembly of the restriction function. Accordingly, *mad3* and *mad4* encode a homolog of the OLD family ABC-ATPases:Toprim nucleases that are also functional in other prokaryotic defense systems (Data S1), where the ATPase activity regulates the nuclease. Here, MAD4 has atypical Toprim motifs, so it may have a function other than DNA cleavage; moreover, around 75% of MADS systems lack *mad3* and *mad4* (Figure 2C), suggesting an auxiliary function. The genes *mad7* and *mad8* encode homologs of the DndG and DndH proteins that form part of the restriction complex of DNA PT-dependent RM systems[34]; MAD7 has an helix-turn-helix (HTH) fold that may recognize unmodified DNA, while MAD8 is a ∼1,800 aa multi-domain protein that includes nuclease and ATPase domains. However, MADS lacks the additional DndF protein. MAD8 could form multimers (either rings or lock-washer assemblies) via its C-terminal HerA/FtsK-like ATPase domain, and this could act as a dsDNA translocase to deliver DNA to the nuclease domain (Figure 6). MAD7 could play a role in distinguishing unmethylated non-self DNA for loading into the MAD8 motor nuclease (Figure 6). The final core protein is MAD6, which has a kinase domain. With analogy to the BREX defense protein

(B) EOP of DMS3*vir* escape mutants (isolated in the experiment shown in A) measured on indicated strains. Individual and mean data are shown for 3 individual biological replicates. Error bars show 95% c.i.

(C) Amplification patterns of DMS3*vir* escape mutants when successively passaged on PA14ΔCRISPR and SMC4386-WT, with the order of passaging indicated on top of the graphs. Phage titer was assessed after each round of amplification using spot assay on PA14ΔCRISPR. Each panel shows data obtained with four independent escape phages (isolated in the experiment shown in A).

(D and E) Each graph shows infection experiments of strains (D) SMC4386ΔCRISPR and (E) SMC4386-WT starting with initial phage concentrations varying from 10^3 to 10^9 PFU/mL (with 10-fold increments) corresponding to initial MOIs ranging from 10^{-4} to 10^2. Red circles highlight replicates where escape phages could be detected. All panels show individual data for 6 independent biological replicates. Details of the statistical tests are provided in Table S2.

CellPress
OPEN ACCESS

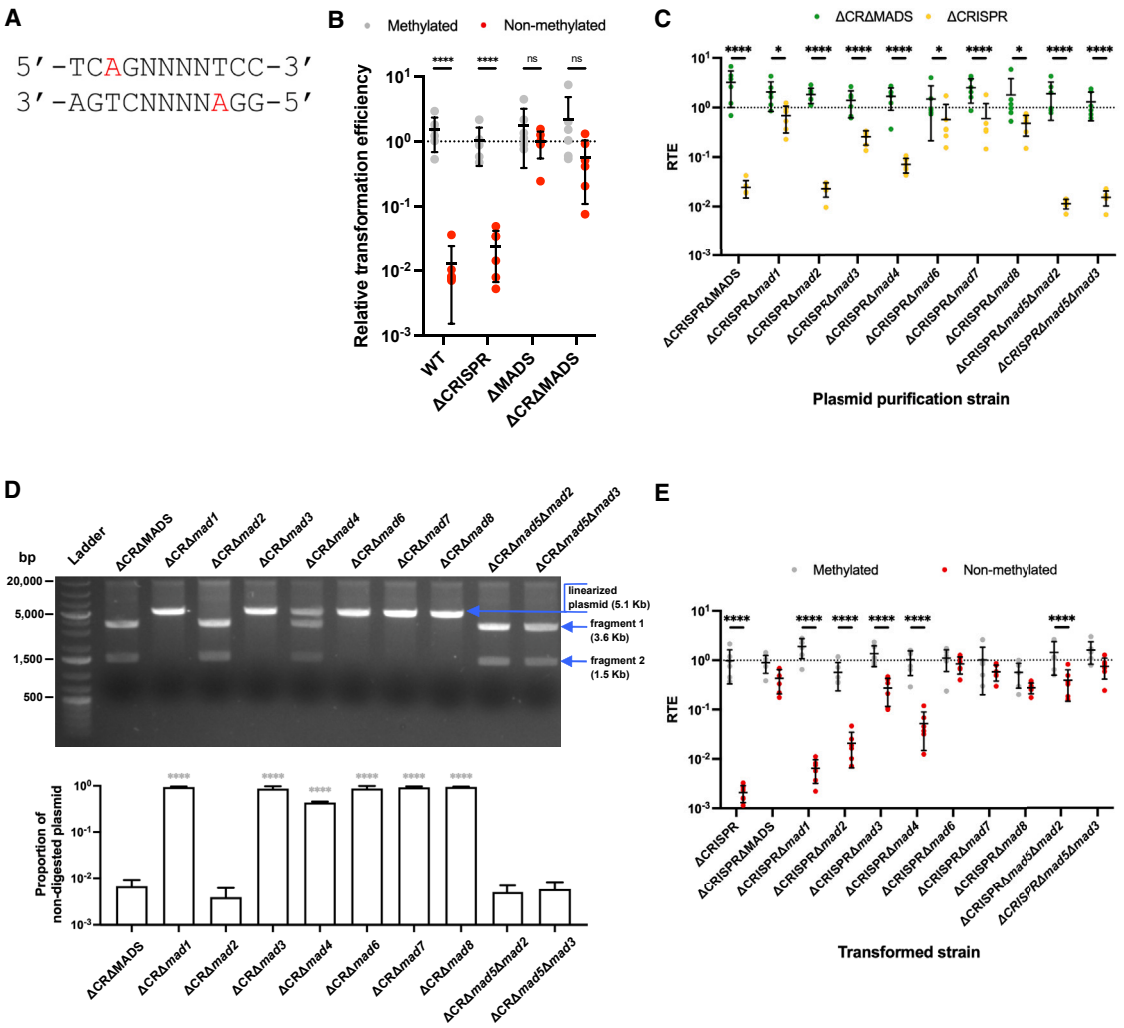

Figure 5. N6-methyladenosine modification of the MADS target sequence abolishes MADS activity

(A) Sequence of the genomic site that is modified by MADS. Adenosines that are methylated at positions 3 and 9 on the positive and negative strands (respectively) are highlighted in red.

(B) Transformation efficiency for methylated (red) or unmethylated (gray) plasmid carrying a 5′-TCAGNNNNTCC-3′ sequence, relative to a plasmid lacking this sequence.

(C) Transformation efficiency of targeted plasmid relative to non-targeted plasmid in ΔCRISPRΔMADS (green) and ΔCRISPR (yellow) strains. The strains used to produce the plasmids ("plasmid purification strain") are indicated along the x axis. Each data point represents an independent biological replicate ($n = 6$), and the mean ± standard deviation (SD) for each treatment is displayed as black bars. Asterisks show differences between RTE in ΔCRISPRΔMADS and ΔCRISPR strains (two-way Anova with Dunnett correction, * $0.01 < p < 0.05$, **** $p < 0.0001$).

(D) (Top) Digestion pattern with NheI (to ensure linearization) and EcoRI of plasmids produced in the indicated strains. Successful digestion with EcoRI produces two fragments of 3.6 and 1.5 kb. Size of the single-digested (i.e., methylated) plasmid is 5.1 kb. (Bottom) Proportion of non-digested (i.e., methylated) plasmids. Strains used for plasmid production are showed in the x axis. Bars represent the mean of 3 independent biological replicate ± SD. Asterisks show differences with plasmid produced in the ΔCRISPRΔMADS strain (one-way Anova with Dunnett correction, **** $p < 0.0001$).

(E) Transformation efficiency of methylated targeted plasmid (gray) and non-methylated (red) targeted plasmid relative to non-targeted plasmid during transformation assay of the strains indicated along the x axis. Each data point represents an independent biological replicate ($n = 6$), and the mean ± SD for each treatment is displayed as black bars. Asterisks show differences between RTE of methylated and non-methylated plasmids (two-way Anova with Dunnett correction, **** $p < 0.0001$). Details of the statistical tests are provided in Table S2.

PglW,[35] MAD6 may sense phage infection, and MADS activity state could be dependent on phosphorylation of key proteins (Figure 6). Mutation of key residues responsible for catalytic phosphorylation (D to N, HRD motif) through site-directed mutagenesis strongly impaired the activity of *mad6*, which was reflected in >10^4-folds reduction in EOP of phage DMS3*vir*, relative to the WT-*mad6* (Figure S1H). Finally, MAD1 could allow transcriptional control that may be important during the establishment of the system or during replication when maintenance methylation is needed to re-modify hemi-methylated sites (Figure 6). Alternatively, it may interact with phage proteins to modulate DNA binding activity (Figure 6).

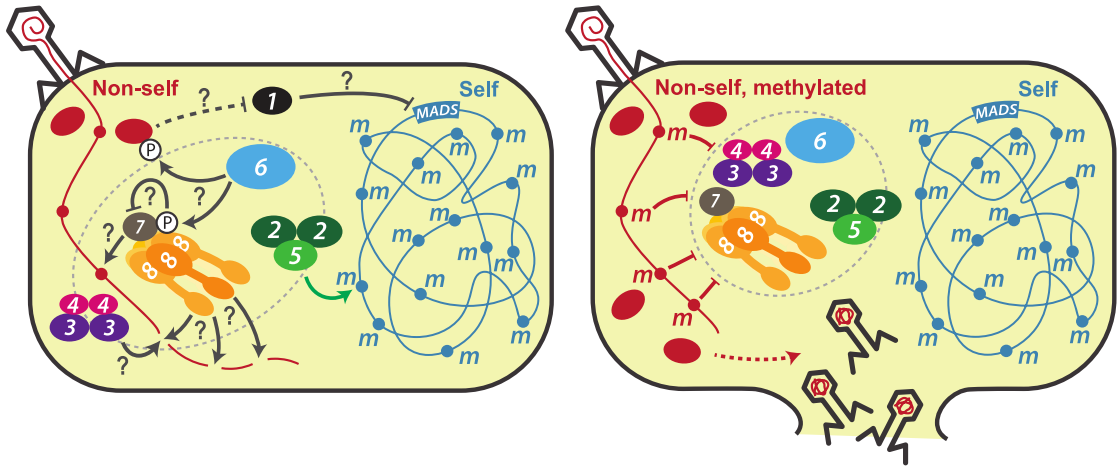

Figure 6. Putative model for MADS modification, restriction, and signaling during infection

Phage-derived proteins are shown as red ovals, and MADS system proteins as numbered ovals. Subunit stoichiometry is based on structural similarity predictions (Data S1). The gray dotted oval indicates that there are likely to be higher-order interactions between the MADS components. DNA is shown as lines (red for phage "non-self" DNA, and blue for bacterial host "self" DNA) with MADS recognition sites (e.g., Figure 5A) as circles with methylated sites marked by an "m." Protein phosphorylation is shown by an encircled "P." Targeting of phage DNA is through recognition of unmodified sites by either MAD7 (shown) or the MAD5:MAD2 N6 methyladenosine MTase (not shown). Question marks next to arrows indicate putative activities that will need to be formally proven by follow up studies. Green arrow indicates the confirmed methylation activity of the MTase. Methylated sites are not targeted by the effector activities, so modified phage sites would provide resistance to restriction (see discussion and Data S1).

DISCUSSION

For the past few years, new defense systems have been discovered at unprecedented rates.[4,7,36] We now understand that bacteria encode many more defense systems than previously thought and that individual bacterial genomes typically contain multiple defenses.[15,28] The most abundant known defense systems are RM and CRISPR-Cas, with a representation of about 80% and 40% in bacterial genomes, respectively.[28] Our bioinformatics investigation revealed that MADS, while being phylogenetically widespread, is also very rare, with a frequency lower than 0.5% in the RefSeq genomes. This is consistent with previous observations that the majority of defense systems are rare, and many more may be awaiting to be discovered.[28] For example, systems such as Tiamat, Nhi, Stk2, Viperin, and Nix1 have all been detected in relatively low proportion of genomes (1.4%, 0.9%, 0.6%, 0.5%, and 0.04%, respectively) (DefenseFinder Wiki | DefenseFinder webservice and knowledge base [mdmlab.fr]), although these numbers may increase as the sensitivity of defense detection tools increases. Out of genomes that carry MADS (706/233,092, 0.3%), we find that 45% also carry a CRISPR-Cas system (total number of all CRISPR hits: 98,120/233,092, 42.1%). However, because the frequency of MADS is generically so low, the overall co-occurrence between MADS and any CRISPR-Cas is also very low (316/233,092, 0.1%). Determining which systems, if any, are present together with MADS in the cases where it is not associated with CRISPR-Cas will be an interesting avenue of inquiry for future studies.

We now know that defense systems are often encoded within MGEs,[37,38] and are commonly enriched in genomic hotspots.[31] The fact that MADS is encoded within a conserved hotspot suggests it could be mobilizable, and it will be interesting to address experimentally in subsequent follow-up investigations whether MADS can be heterologously transferred to different bacterial species and provide resistance to MGE infections.

Most defense systems have a relatively simple genetic makeup, often consisting of a single gene for infection sensing and a single effector gene for interference (Table S5). In comparison, MADS is highly complex, consisting of an 8 gene operon of over 17 kb. Its genetic architecture and domain content point toward more elaborate mechanisms of sensing infection, defense activation, and/or interference, as seen in other genetically more complex systems such as Dpd, BREX, and CRISPR-Cas.

Our genetic analyses have identified the *mads* genes involved in self/non-self discrimination, which is based on N6-methyladenosine modification of a specific recognition sequence, which is similar to self/non-self discrimination by RM, defense island system associated with restriction modification (DISARM), BREX, and phage growth limitation (Pgl) systems. While this is a common feature shared with the aforementioned systems, it is noted that, unlike RM, MADS functionality and regulation rely on additional proteins, such as MAD1 and MAD6 at least based on the current knowledge. Whether MADS and perhaps other recently discovered defense systems will form a divergence or subtype within a bigger group will be clarified by future studies and updates on the current system descriptions and classifications.

Our protein structure analyses suggest that at least two components of MADS have the potential to be ATPase-switched nucleases that could target unmodified phage DNA, possibly controlled by the kinase and winged HTH proteins to ensure activity to be turned on during infection. It is likely that some of the MADS encoded proteins may assemble in large multiprotein complexes (Figure 6) and that domains such as the S/T kinase and HTH could play a role in regulation of defense

activity—hypotheses that need to be addressed in future biochemical studies.

Interestingly, while phages readily acquired epigenetic modifications to overcome MADS alone, the co-existence of MADS and CRISPR-Cas immunity prevented the emergence and spread of escape phages, even though the phage carries an *acr* counter-defense gene. This supports the more general idea that multi-layered defenses of bacteria provide more durable protection against rapidly evolving phages.[39] For example, recent studies showed that the co-occurrence of a type I BREX and type IV RM systems prevents the emergence of epigenetic mutants that overcome BREX since these are cleaved by the type IV RM system,[40] and that the co-existence of RM and CRISPR-Cas leads to a reduction in the frequency of spontaneous phage mutants that escape both defenses, as well as a higher rate of CRISPR immunity acquisition.[16–18] Moreover, it was recently found that RM and type VI CRISPR-Cas systems, which induce a dormancy response[41] frequently co-occur and synergize to clear phage infections and resuscitate cells.[42] In the case of the MADS-CRISPR-Cas interaction reported here, we find that Acr-phages rapidly fall below the limit of detection because unmodified phages are unable to infect bacteria due to MADS activity, whereas MADS escape phages are too rare in the population to successfully cooperate to overcome CRISPR immunity. Hence, our data show that multi-layered defenses not only provide effective barriers against mutation-based evasion of immune systems but can also interfere with successful deployment of phage-encoded counter-defense genes.

STAR★METHODS

Detailed methods are provided in the online version of this paper and include the following:

- KEY RESOURCES TABLE
- RESOURCE AVAILABILITY
  - Lead contact
  - Materials availability
  - Data and code availability
- EXPERIMENTAL MODEL AND SUBJECT DETAILS
  - Bacterial strains
  - Phage strains
- METHOD DETAILS
  - Adsorption assay
  - Efficiency of Plaquing (EOP) assays
  - Generation of the transposon (Tn)-mutant library
  - Measuring frequencies of lysogeny
  - Localization of the Tn5 insertions
  - Generation of gene knockouts
  - Growth curves
  - Construction of pLola plasmids
  - Complementation assay
  - Bioinformatic analysis of the distribution of MADS
  - Bioinformatic analysis of defense islands
  - Analysis of MADS self/non-self discrimination
  - CRISPR immunosuppression assay
  - Plasmid transformation assays – Methylation pattern
  - Plasmid *in vitro* digestion assay
  - Plasmid transformation assays – Restriction pattern
  - Phenotypic interactions between CRISPR-Cas and MADS
  - Site directed mutagenesis
  - Mathematical modelling
- QUANTIFICATION AND STATYSTICAL ANALYSIS

SUPPLEMENTAL INFORMATION

Supplemental information can be found online at https://doi.org/10.1016/j.chom.2024.07.005.

ACKNOWLEDGMENTS

The authors thank Dr. L. Zhang for his support in optimizing the protocol for arbitrary PCR, Dr. D. Sünderhauf for assistance in generating the transposon-mutant library, Dr. B. Watson for contributing to phage DNA isolation, Dr. A. Bernheim for feedback on building macromolecular models to detect MADS, E. Cenraud for DefenseFinder analyses, Prof. R. Lavigne and Dr. J. Wagemans for kindly providing phage LPB1, Prof. Michael Brockhurst and Dr. R. Wright for kindly providing phage PA14P2, Prof. O'Toole for kindly providing phage DMS3*vir* and strain *P. aeruginosa* UCBPP-PA14 *csy3::lacZ*, Prof. Davidson and Prof. Bondy-Denomy for kindly providing strain SMC4386 and phage JBD25, and Dr. S. Jackson for kindly sharing the PADLOC outputs for the RefSeq genomes. Funding: PhD studentship sponsored by the College of Life and Environmental Sciences, University of Exeter, and the Centre for Environment, Fisheries and Aquaculture Science supported A.M.; UK Research and Innovation under the UK Government's Horizon Europe funding guarantee EP/Y020308/1 (awarded to A.A.); European Research Council—European Union's Horizon2020 research and innovation programme ERC-2017-ADG-788405 (awarded to M.D.S.); Medical Research Council MR/R020787/1 (awarded to K.S.B.); Biotechnology and Biological Sciences Research Council BB/S017674/1 (awarded to S.v.H.); UK Research and Innovation grant under the UK Government's Horizon Europe funding guarantee EP/X026507/1 (awarded to S.v.H.); European Union's Horizon 2020 research and innovation programme—Marie Skłodowska-Curie grant agreement no 834052 (awarded to A.C.); IdEx Université Paris Cité ANR 18 IDEX 0001 (awarded to A.C.); Biotechnology and Biological Sciences Research Council sLoLa BB/X003051/1 (awarded to M.D.S., K.S.B., S.v.H., and E.R.W.); European Research Council—European Union's Horizon2020 research and innovation programme ERC-STG-2016-714478 (awarded to E.R.W.). For the purpose of open access, the author has applied a Creative Commons Attribution (CC BY) license to any Author Accepted Manuscript version arising from this submission.

AUTHOR CONTRIBUTIONS

Conceptualization: A.M., A.C., and E.R.W.; methodology: A.M., B.J.P., E.P., C.E.C., S.G., A.O., A.A., M.D.S., K.S.B., A.C., and E.R.W.; investigation: A.M., B.J.P., E.P., C.E.C., S.G., R.C., A.O., A.A., M.A.W.C., A.G., S.P., M.D.S., K.S.B., S.v.H., A.C., and E.R.W.; mathematical modelling: S.G.; structural modelling: M.D.S.; bioinformatics—MacsyFinder model: E.P.; bioinformatics—defense islands: A.M., C.E.C., K.S.B., and A.C.; writing—original draft: A.M., A.C., and E.R.W.; writing—review & editing: A.M., B.J.P., E.P., C.E.C., S.G., R.C., A.O., A.A., M.A.W.C., S.P., M.D.S., K.S.B., S.v.H., A.C., and E.R.W.; supervision: A.C. and E.R.W.; funding acquisition: E.R.W.

DECLARATION OF INTERESTS

A.M., A.C., and E.R.W. are inventors on patent GB2303034.9.

Received: August 9, 2023
Revised: April 23, 2024
Accepted: July 8, 2024
Published: August 1, 2024

REFERENCES

1. Chevallereau, A., Pons, B.J., van Houte, S., and Westra, E.R. (2022). Interactions between bacterial and phage communities in natural environments. Nat. Rev. Microbiol. *20*, 49–62. https://doi.org/10.1038/s41579-021-00602-y.
2. Mayo-Muñoz, D., Pinilla-Redondo, R., Birkholz, N., and Fineran, P.C. (2023). A host of armor: Prokaryotic immune strategies against mobile

genetic elements. Cell Rep. *42*, 112672. https://doi.org/10.1016/j.celrep.2023.112672.

3. Millman, A., Melamed, S., Leavitt, A., Doron, S., Bernheim, A., Hör, J., Lopatina, A., Ofir, G., Hochhauser, D., Stokar-Avihail, A., et al. (2022). An expanding arsenal of immune systems that protect bacteria from phages. Cell Host Microbe *30*, 1556–1569.e5. https://doi.org/10.1101/2022.05.11.491447.
4. Doron, S., Melamed, S., Ofir, G., Leavitt, A., Lopatina, A., Keren, M., Amitai, G., and Sorek, R. (2018). Systematic discovery of antiphage defense systems in the microbial pangenome. Science *359*, eaar4120. https://doi.org/10.1126/science.aar4120.
5. Cohen, D., Melamed, S., Millman, A., Shulman, G., Oppenheimer-Shaanan, Y., Kacen, A., Doron, S., Amitai, G., and Sorek, R. (2019). Cyclic GMP–AMP signalling protects bacteria against viral infection. Nature *574*, 691–695. https://doi.org/10.1038/s41586-019-1605-5.
6. Millman, A., Bernheim, A., Stokar-Avihail, A., Fedorenko, T., Voichek, M., Leavitt, A., Oppenheimer-Shaanan, Y., and Sorek, R. (2020). Bacterial Retrons Function In Anti-Phage Defense. Cell *183*, 1551–1561.e12. https://doi.org/10.1016/j.cell.2020.09.065.
7. Gao, L., Altae-Tran, H., Böhning, F., Makarova, K.S., Segel, M., Schmid-Burgk, J.L., Koob, J., Wolf, Y.I., Koonin, E.V., and Zhang, F. (2020). Diverse enzymatic activities mediate antiviral immunity in prokaryotes. Science *369*, 1077–1084. https://doi.org/10.1126/science.aba0372.
8. Tal, N., Morehouse, B.R., Millman, A., Stokar-Avihail, A., Avraham, C., Fedorenko, T., Yirmiya, E., Herbst, E., Brandis, A., Mehlman, T., et al. (2021). Cyclic CMP and cyclic UMP mediate bacterial immunity against phages. Cell *184*, 5728–5739.e16. https://doi.org/10.1016/j.cell.2021.09.031.
9. Bernheim, A., Millman, A., Ofir, G., Meitav, G., Avraham, C., Shomar, H., Rosenberg, M.M., Tal, N., Melamed, S., Amitai, G., and Sorek, R. (2021). Prokaryotic viperins produce diverse antiviral molecules. Nature *589*, 120–124. https://doi.org/10.1038/s41586-020-2762-2.
10. Makarova, K.S., Wolf, Y.I., Snir, S., and Koonin, E.V. (2011). Defense Islands in Bacterial and Archaeal Genomes and Prediction of Novel Defense Systems. J. Bacteriol. *193*, 6039–6056. https://doi.org/10.1128/JB.05535-11.
11. Makarova, K.S., Wolf, Y.I., and Koonin, E.V. (2013). Comparative genomics of defense systems in archaea and bacteria. Nucleic Acids Res. *41*, 4360–4377. https://doi.org/10.1093/nar/gkt157.
12. Bari, S.M.N., Chou-Zheng, L., Howell, O., Hossain, M., Hill, C.M., Boyle, T.A., Cater, K., Dandu, V.S., Thomas, A., Aslan, B., and Hatoum-Aslan, A. (2022). A unique mode of nucleic acid immunity performed by a multifunctional bacterial enzyme. Cell Host Microbe *30*, 570–582.e7. https://doi.org/10.1016/j.chom.2022.03.001.
13. Barrangou, R., Fremaux, C., Deveau, H., Richards, M., Boyaval, P., Moineau, S., Romero, D.A., and Horvath, P. (2007). CRISPR Provides Acquired Resistance Against Viruses in Prokaryotes. Science *315*, 1709–1712. https://doi.org/10.1126/science.1138140.
14. Bernheim, A., and Sorek, R. (2020). The pan-immune system of bacteria: antiviral defence as a community resource. Nat. Rev. Microbiol. *18*, 113–119. https://doi.org/10.1038/s41579-019-0278-2.
15. Oliveira, P.H., Touchon, M., and Rocha, E.P.C. (2014). The interplay of restriction-modification systems with mobile genetic elements and their prokaryotic hosts. Nucleic Acids Res. *42*, 10618–10631. https://doi.org/10.1093/nar/gku734.
16. Dupuis, M.-È., Villion, M., Magadán, A.H., and Moineau, S. (2013). CRISPR-Cas and restriction–modification systems are compatible and increase phage resistance. Nat. Commun. *4*, 2087. https://doi.org/10.1038/ncomms3087.
17. Hynes, A.P., Villion, M., and Moineau, S. (2014). Adaptation in bacterial CRISPR-Cas immunity can be driven by defective phages. Nat. Commun. *5*, 4399. https://doi.org/10.1038/ncomms5399.
18. Maguin, P., Varble, A., Modell, J.W., and Marraffini, L.A. (2022). Cleavage of viral DNA by restriction endonucleases stimulates the type II CRISPR-Cas immune response. Mol. Cell *82*, 907–919.e7. https://doi.org/10.1016/j.molcel.2022.01.012.
19. Spoerel, N., Herrlich, P., and Bickle, T.A. (1979). A novel bacteriophage defence mechanism: the anti-restriction protein. Nature *278*, 30–34. https://doi.org/10.1038/278030a0.
20. Bondy-Denomy, J., Pawluk, A., Maxwell, K.L., and Davidson, A.R. (2013). Bacteriophage genes that inactivate the CRISPR/Cas bacterial immune system. Nature *493*, 429–432. https://doi.org/10.1038/nature11723.
21. Huiting, E., Athukoralage, J., Guan, J., Silas, S., Carion, H., and Bondy-Denomy, J. (2022). Bacteriophages antagonize cGAS-like immunity in bacteria. Preprint at bioRxiv. https://doi.org/10.1101/2022.03.30.486325.
22. Hobbs, S.J., Wein, T., Lu, A., Morehouse, B.R., Schnabel, J., Leavitt, A., Yirmiya, E., Sorek, R., and Kranzusch, P.J. (2022). Phage anti-CBASS and anti-Pycsar nucleases subvert bacterial immunity. Nature *605*, 522–526. https://doi.org/10.1038/s41586-022-04716-y.
23. Ho, P., Chen, Y., Biswas, S., Canfield, E., Abdolvahabi, A., and Feldman, D.E. (2023). Bacteriophage antidefense genes that neutralize TIR and STING immune responses. Cell Rep. *42*, 112305. https://doi.org/10.1016/j.celrep.2023.112305.
24. Borges, A.L., Zhang, J.Y., Rollins, M.F., Osuna, B.A., Wiedenheft, B., and Bondy-Denomy, J. (2018). Bacteriophage Cooperation Suppresses CRISPR-Cas3 and Cas9 Immunity. Cell *174*, 917–925.e10. https://doi.org/10.1016/j.cell.2018.06.013.
25. Landsberger, M., Gandon, S., Meaden, S., Rollie, C., Chevallereau, A., Chabas, H., Buckling, A., Westra, E.R., and van Houte, S. (2018). Anti-CRISPR Phages Cooperate to Overcome CRISPR-Cas Immunity. Cell *174*, 908–916.e12. https://doi.org/10.1016/j.cell.2018.05.058.
26. Pawluk, A., Bondy-Denomy, J., Cheung, V.H.W., Maxwell, K.L., and Davidson, A.R. (2014). A New Group of Phage Anti-CRISPR Genes Inhibits the Type I-E CRISPR-Cas System of Pseudomonas aeruginosa. mBio *5*, e00896. https://doi.org/10.1128/mBio.00896-14.
27. Payne, L.J., Meaden, S., Mestre, M.R., Palmer, C., Toro, N., Fineran, P.C., and Jackson, S.A. (2022). PADLOC: a web server for the identification of antiviral defence systems in microbial genomes. Nucleic Acids Res. *50*, W541–W550. https://doi.org/10.1093/nar/gkac400.
28. Tesson, F., Hervé, A., Mordret, E., Touchon, M., d'Humières, C., Cury, J., and Bernheim, A. (2022). Systematic and quantitative view of the antiviral arsenal of prokaryotes. Nat. Commun. *13*, 2561. https://doi.org/10.1038/s41467-022-30269-9.
29. Hockenberry, A.J., and Wilke, C.O. (2021). BACPHLIP: predicting bacteriophage lifestyle from conserved protein domains. PeerJ *9*, e11396. https://doi.org/10.7717/peerj.11396.
30. Abby, S.S., Néron, B., Ménager, H., Touchon, M., and Rocha, E.P.C. (2014). MacSyFinder: A Program to Mine Genomes for Molecular Systems with an Application to CRISPR-Cas Systems. PLoS ONE *9*, e110726. https://doi.org/10.1371/journal.pone.0110726.
31. Johnson, M.C., Laderman, E., Huiting, E., Zhang, C., Davidson, A., and Bondy-Denomy, J. (2023). Core defense hotspots within Pseudomonas aeruginosa are a consistent and rich source of anti-phage defense systems. Nucleic Acids Res. *51*, 4995–5005. https://doi.org/10.1093/nar/gkad317.
32. Hampton, H.G., Watson, B.N.J., and Fineran, P.C. (2020). The arms race between bacteria and their phage foes. Nature *577*, 327–336. https://doi.org/10.1038/s41586-019-1894-8.
33. Loenen, W.A.M., Dryden, D.T.F., Raleigh, E.A., and Wilson, G.G. (2014). Type I restriction enzymes and their relatives. Nucleic Acids Res. *42*, 20–44. https://doi.org/10.1093/nar/gkt847.
34. Wu, D., Tang, Y., Chen, S., He, Y., Chang, X., Zheng, W., Deng, Z., Li, Z., Wang, L., Wu, G., and Chen, S. (2022). The functional coupling between restriction and DNA phosphorothioate modification systems underlying

the DndFGH restriction complex. Nat. Catal. *5*, 1131–1144. https://doi.org/10.1038/s41929-022-00884-2.

35. Hoskisson, P.A., Sumby, P., and Smith, M.C.M. (2015). The phage growth limitation system in Streptomyces coelicolor A(3)2 is a toxin/antitoxin system, comprising enzymes with DNA methyltransferase, protein kinase and ATPase activity. Virology *477*, 100–109. https://doi.org/10.1016/j.virol.2014.12.036.

36. Georjon, H., and Bernheim, A. (2023). The highly diverse antiphage defence systems of bacteria. Nat. Rev. Microbiol. *21*, 686–700. https://doi.org/10.1038/s41579-023-00934-x.

37. Rousset, F., Depardieu, F., Miele, S., Dowding, J., Laval, A.-L., Lieberman, E., Garry, D., Rocha, E.P.C., Bernheim, A., and Bikard, D. (2022). Phages and their satellites encode hotspots of antiviral systems. Cell Host Microbe *30*, 740–753.e5. https://doi.org/10.1016/j.chom.2022.02.018.

38. Patel, P.H., and Maxwell, K.L. (2023). Prophages provide a rich source of antiphage defense systems. Curr. Opin. Microbiol. *73*, 102321. https://doi.org/10.1016/j.mib.2023.102321.

39. Gandon, S., Guillemet, M., Gatchitch, F., Nicot, A., Renaud, A.C., Tremblay, D.M., and Moineau, S. (2024). Building pyramids against the evolutionary emergence of pathogens. Proc. Biol. Sci. *291*, 20231529. https://doi.org/10.1098/rspb.2023.1529.

40. Picton, D.M., Luyten, Y.A., Morgan, R.D., Nelson, A., Smith, D.L., Dryden, D.T.F., Hinton, J.C.D., and Blower, T.R. (2021). The phage defence island of a multidrug resistant plasmid uses both BREX and type IV restriction for complementary protection from viruses. Nucleic Acids Res. *49*, 11257–11273. https://doi.org/10.1093/nar/gkab906.

41. Meeske, A.J., Nakandakari-Higa, S., and Marraffini, L.A. (2019). Cas13-induced cellular dormancy prevents the rise of CRISPR-resistant bacteriophage. Nature *570*, 241–245. https://doi.org/10.1038/s41586-019-1257-5.

42. Williams, M.C., Reker, A.E., Margolis, S.R., Liao, J., Wiedmann, M., Rojas, E.R., and Meeske, A.J. (2023). Restriction endonuclease cleavage of phage DNA enables resuscitation from Cas13-induced bacterial dormancy. Nat. Microbiol. *8*, 400–409. https://doi.org/10.1038/s41564-022-01318-2.

43. Cady, K.C., Bondy-Denomy, J., Heussler, G.E., Davidson, A.R., and O'Toole, G.A. (2012). The CRISPR/Cas Adaptive Immune System of Pseudomonas aeruginosa Mediates Resistance to Naturally Occurring and Engineered Phages. J. Bacteriol. *194*, 5728–5738. https://doi.org/10.1128/JB.01184-12.

44. Stover, C.K., Pham, X.Q., Erwin, A.L., Mizoguchi, S.D., Warrener, P., Hickey, M.J., Brinkman, F.S.L., Hufnagle, W.O., Kowalik, D.J., Lagrou, M., et al. (2000). Complete genome sequence of Pseudomonas aeruginosa PAO1, an opportunistic pathogen. Nature *406*, 959–964. https://doi.org/10.1038/35023079.

45. Blattner, F.R., Plunkett, G., Bloch, C.A., Perna, N.T., Burland, V., Riley, M., Collado-Vides, J., Glasner, J.D., Rode, C.K., Mayhew, G.F., et al. (1997). The complete genome sequence of Escherichia coli K-12. Science *277*, 1453–1462. https://doi.org/10.1126/science.277.5331.1453.

46. Ferrières, L., Hémery, G., Nham, T., Guérout, A.-M., Mazel, D., Beloin, C., and Ghigo, J.-M. (2010). Silent Mischief: Bacteriophage Mu Insertions Contaminate Products of *Escherichia coli* Random Mutagenesis Performed Using Suicidal Transposon Delivery Plasmids Mobilized by Broad-Host-Range RP4 Conjugative Machinery. J. Bacteriol. *192*, 6418–6427. https://doi.org/10.1128/JB.00621-10.

47. Simon, R., Priefer, U., and Pühler, A. (1983). A Broad Host Range Mobilization System for In Vivo Genetic Engineering: Transposon Mutagenesis in Gram Negative Bacteria. Nat. Biotechnol. *1*, 784–791. https://doi.org/10.1038/nbt1183-784.

48. Chevallereau, A., Meaden, S., Fradet, O., Landsberger, M., Maestri, A., Biswas, A., Gandon, S., van Houte, S., and Westra, E.R. (2020). Exploitation of the Cooperative Behaviors of Anti-CRISPR Phages. Cell Host Microbe *27*, 189–198.e6. https://doi.org/10.1016/j.chom.2019.12.004.

49. Wright, R.C.T., Friman, V.-P., Smith, M.C.M., and Brockhurst, M.A. (2018). Cross-resistance is modular in bacteria–phage interactions. PLOS Biol. *16*, e2006057. https://doi.org/10.1371/journal.pbio.2006057.

50. Mattila, S., Ruotsalainen, P., and Jalasvuori, M. (2015). On-Demand Isolation of Bacteriophages Against Drug-Resistant Bacteria for Personalized Phage Therapy. Front. Microbiol. *6*, 1271. https://doi.org/10.3389/fmicb.2015.01271.

51. Martínez-García, E., Aparicio, T., de Lorenzo, V., and Nikel, P.I. (2014). New Transposon Tools Tailored for Metabolic Engineering of Gram-Negative Microbial Cell Factories. Front. Bioeng. Biotechnol. *2*, 46. https://doi.org/10.3389/fbioe.2014.00046.

52. Hmelo, L.R., Borlee, B.R., Almblad, H., Love, M.E., Randall, T.E., Tseng, B.S., Lin, C., Irie, Y., Storek, K.M., Yang, J.J., et al. (2015). Precision-engineering the Pseudomonas aeruginosa genome with two-step allelic exchange. Nat. Protoc. *10*, 1820–1841. https://doi.org/10.1038/nprot.2015.115.

53. Seemann, T. (2014). Prokka: rapid prokaryotic genome annotation. Bioinformatics *30*, 2068–2069. https://doi.org/10.1093/bioinformatics/btu153.

54. Quinlan, A.R., and Hall, I.M. (2010). BEDTools: a flexible suite of utilities for comparing genomic features. Bioinformatics *26*, 841–842. https://doi.org/10.1093/bioinformatics/btq033.

55. Cock, P.J.A., Antao, T., Chang, J.T., Chapman, B.A., Cox, C.J., Dalke, A., Friedberg, I., Hamelryck, T., Kauff, F., Wilczynski, B., and de Hoon, M.J. (2009). Biopython: freely available Python tools for computational molecular biology and bioinformatics. Bioinformatics *25*, 1422–1423. https://doi.org/10.1093/bioinformatics/btp163.

56. Waterhouse, A.M., Procter, J.B., Martin, D.M.A., Clamp, M., and Barton, G.J. (2009). Jalview Version 2 - A multiple sequence alignment editor and analysis workbench. Bioinformatics *25*, 1189–1191. https://doi.org/10.1093/bioinformatics/btp033.

57. Kelley, L.A., Mezulis, S., Yates, C.M., Wass, M.N., and Sternberg, M.J.E. (2015). The Phyre2 web portal for protein modeling, prediction and analysis. Nat. Protoc. *10*, 845–858. https://doi.org/10.1038/nprot.2015.053.

58. M.R.J. Clokie, and A.M. Kropinski, eds. (2009). Bacteriophages (Humana Press). https://doi.org/10.1007/978-1-60327-164-6.

59. Martínez-García, E., Calles, B., Arévalo-Rodríguez, M., and de Lorenzo, V. (2011). pBAM1: an all-synthetic genetic tool for analysis and construction of complex bacterial phenotypes. BMC Microbiol. *11*, 38. https://doi.org/10.1186/1471-2180-11-38.

60. Saavedra, J.T., Schwartzman, J.A., and Gilmore, M.S. (2017). Mapping Transposon Insertions in Bacterial Genomes by Arbitrarily Primed PCR. Curr. Protoc. Mol. Biol. *118*, 15.15.1–15.15.15. https://doi.org/10.1002/cpmb.38.

61. Horton, R.M., Hunt, H.D., Ho, S.N., Pullen, J.K., and Pease, L.R. (1989). Engineering hybrid genes without the use of restriction enzymes: gene splicing by overlap extension. Gene *77*, 61–68. https://doi.org/10.1016/0378-1119(89)90359-4.

62. Horton, R.M., Cai, Z., Ho, S.N., and Pease, L.R. (2013). Gene Splicing by Overlap Extension: Tailor-Made Genes Using the Polymerase Chain Reaction. BioTechniques *54*, 129–133. https://doi.org/10.2144/000114017.

63. Zimmermann, L., Stephens, A., Nam, S.-Z., Rau, D., Kübler, J., Lozajic, M., Gabler, F., Söding, J., Lupas, A.N., and Alva, V. (2018). A Completely Reimplemented MPI Bioinformatics Toolkit with a New HHpred Server at its Core. J. Mol. Biol. *430*, 2237–2243. https://doi.org/10.1016/j.jmb.2017.12.007.

64. Altschul, S.F., Gish, W., Miller, W., Myers, E.W., and Lipman, D.J. (1990). Basic Local Alignment Search Tool. J. Mol. Biol. *215*, 403–410. https://doi.org/10.1016/S0022-2836(05)80360-2.

65. Pons, B.J., Westra, E.R., and van Houte, S. (2023). Determination of Acr-mediated immunosuppression in Pseudomonas aeruginosa. MethodsX *10*, 101941. https://doi.org/10.1016/j.mex.2022.101941.

66. Strong, T.C., Kaur, G., and Thomas, J.H. (2011). Mutations in the Catalytic Loop HRD Motif Alter the Activity and Function of Drosophila Src64. PLOS ONE *6*, e28100. https://doi.org/10.1371/journal.pone.0028100.

67. Williams, D.M., and Cole, P.A. (2002). Proton Demand Inversion in a Mutant Protein Tyrosine Kinase Reaction. J. Am. Chem. Soc. *124*, 5956–5957. https://doi.org/10.1021/ja025993a.

68. Taylor, S.S., and Kornev, A.P. (2011). Protein kinases: evolution of dynamic regulatory proteins. Trends Biochem. Sci. *36*, 65–77. https://doi.org/10.1016/j.tibs.2010.09.006.

69. Hanks, S.K., Quinn, A.M., and Hunter, T. (1988). The Protein Kinase Family: Conserved Features and Deduced Phylogeny of the Catalytic Domains. Science *241*, 42–52. https://doi.org/10.1126/science.3291115.

70. Adams, J.A. (2001). Kinetic and catalytic mechanisms of protein kinases. Chem. Rev. *101*, 2271–2290. https://doi.org/10.1021/cr000230w.

STAR★METHODS

KEY RESOURCES TABLE

REAGENT or RESOURCE	SOURCE	IDENTIFIER
Bacterial and Virus Strains		
P. aeruginosa SMC4386	Davidson Lab, Pawluk et al.[26]	NCBI: NZ_LOQZ00000000.1
P. aeruginosa SMC4386ΔCRISPR	Westra Lab, this study	N/A
P. aeruginosa SMC4386ΔMADS	Westra Lab, this study	N/A
P. aeruginosa SMC4386ΔCRISPRΔMADS	Westra Lab, this study	N/A
P. aeruginosa SMC4386Δ*mad1*	Westra Lab, this study	N/A
P. aeruginosa SMC4386Δ*mad2*	Westra Lab, this study	N/A
P. aeruginosa SMC4386Δ*mad3*	Westra Lab, this study	N/A
P. aeruginosa SMC4386Δ*mad4*	Westra Lab, this study	N/A
P. aeruginosa SMC4386Δ*mad6*	Westra Lab, this study	N/A
P. aeruginosa SMC4386Δ*mad7*	Westra Lab, this study	N/A
P. aeruginosa SMC4386Δ*mad8*	Westra Lab, this study	N/A
P. aeruginosa SMC4386Δ*mad2Δmad5*	Westra Lab, this study	N/A
P. aeruginosa SMC4386Δ*mad3Δmad5*	Westra Lab, this study	N/A
P. aeruginosa UCBPP-PA14 csy3::LacZ	O'Toole Lab, Cady et al.[43]	N/A
P. aeruginosa PAO1	Stover et al. [44]	NCBI: NC_002516
E. coli MG1655	Blattner et al.[45]	N/A
E. coli MFD*pir*	Ferrières et al.[46]	N/A
E. coli DH5α	Thermo Fisher Scientific	Cat#18265017
E. coli S17-1λ*pir*	Simon et al.[47]	N/A
Pseudomonas Phage DMS3-gmR	Bondy-Denomy Lab, Borges et al.[24]	N/A
Pseudomonas Phage DMS3*vir*	O'Toole Lab, Cady et al.[43]	N/A
Pseudomonas Phage DMS3*virΔacr*	Westra Lab, Chevallereau et al.[48]	N/A
Pseudomonas Phage LPB1	Lavigne Lab	RefSeq: NC_027298.1
Pseudomonas Phage PA14P2	Brockhurst Lab, Wright et al.[49] (see also Mattila et al.[50])	N/A
Pseudomonas Phage JBD25	Davidson Lab, Cady et al.[43]	NCBI:txid1225792
Critical Commercial Assays		
Thermo Scientific GeneJET Plasmid MiniPrep Kit	Fisher	Cat #01078644 (K0503)
QIAquick Gel Extraction Kit	QIAGEN	#28506
Gateway BP Clonase II Enzyme Mix	Fisher	#2049500
Q5-Site Directed Mutagenesis Kit	NEB	E0554
NEBuilder HiFi DNA Assembly Cloning Kit	NEB	Cat #E5520S
Deposited Data		
Sequencing Data	This study	NCBI: PRJEB61545
Source Data	This study	https://github.com/alicemaestri/raw_data_MADS_CHM
Bacterial and Archaeal RefSeq Assemblies and Scripts	This study	https://github.com/elliekpursey/Maestri
Oligonucleotides		
Primers for Transposon-Library Assay	IDT	Table S6
Primers for Gene Deletion Assays	IDT	Table S6
Primers for Targeted Plasmid Construction	IDT	Table S6
Primers for pLola Plasmids Construction and Complementation Assay	IDT	Table S6
Primers for Site Directed Mutagenesis	IDT	Table S6

(*Continued on next page*)

Continued

REAGENT or RESOURCE	SOURCE	IDENTIFIER
Primers for Construction of pLola Plasmids	IDT	Table S6
Recombinant DNA		
pBAMD1-4	Martínez-García et al.[51]	GeneBank: KM403114
pDONRPEX18Gm	Hmelo et al.[52]	GeneBank: KM880128.1
pDONRPEX18Gm-CRISPR-KO	Westra Lab, this study	N/A
pDONRPEX18Gm-MADS-KO	Westra Lab, this study	N/A
pDONRPEX18Gm-*mad1*-KO	Westra Lab, this study	N/A
pDONRPEX18Gm-*mad2*-KO	Westra Lab, this study	N/A
pDONRPEX18Gm-*mad3*-KO	Westra Lab, this study	N/A
pDONRPEX18Gm-*mad4*-KO	Westra Lab, this study	N/A
pDONRPEX18Gm-*mad5*-KO	Westra Lab, this study	N/A
pDONRPEX18Gm-*mad6*-KO	Westra Lab, this study	N/A
pDONRPEX18Gm-*mad7*-KO	Westra Lab, this study	N/A
pDONRPEX18Gm-*mad8*-KO	Westra Lab, this study	N/A
pHERD30T	Bondy-Denomy et al.[20]	GenBank: EU603326.1
pHERD30T- cr1sp2-SMC	Westra Lab, this study	N/A
pHERD30T-M24	Westra Lab, this study	N/A
pHERD30T-MADS-EcoRI	Westra Lab, this study	N/A
pHERD30T-Nonmeth	Westra Lab, this study	N/A
pHERD30T-M24-Nonmeth	Westra Lab, this study	N/A
pHERD30T-Meth	Westra Lab, this study	N/A
pHERD30T-M24-Meth	Westra Lab, this study	N/A
pLola-*mad1*-RhaP	Westra Lab, this study	N/A
pLola-*mad2*-RhaP	Westra Lab, this study	N/A
pLola-*mad3*-RhaP	Westra Lab, this study	N/A
pLola-*mad4*-MADSP	Westra Lab, this study	N/A
pLola-*mad6*-MADSP	Westra Lab, this study	N/A
pLola-*mad6*-HRDmut-MADSP	Westra Lab, this study	N/A
pLola-*mad7*-RhaP	Westra Lab, this study	N/A
pLola-mCherry-RhaP	Westra Lab, this study	N/A
pLola-mCherry-MADSP	Westra Lab, this study	N/A
Software and Algorithms		
Geneious version 10.2.6	Biomatters	https://www.geneious.com
R version 4.0.4	R Core Team, 2014	https://www.R-project.org/
R version 4.1.3	R Core Team, 2014	https://www.R-project.org/
Prism 8.3.0	Graph Pad	https://www.graphpad.com/scientific-software/prism/
Prokka version 1.14.6	Seemann[53]	https://github.com/tseemann/prokka
BEDTools version 2.29.2	Quinlan, A.R., and Hall[54]	https://github.com/arq5x/bedtools2
PADLOC	Payne et al.[27]	https://padloc.otago.ac.nz/padloc/
DefenseFinder	Tesson et al.[28]	https://defense-finder.mdmparis-lab.com
MacSyFinder version 2	Abby et al.[30]	https://github.com/gem-pasteur/macsyfinder
HMMER version 3.0	HMMER development team	http://hmmer.org/
Python Version 3.9.7	Python Software Foundation	https://www.python.org/
Biopython version 1.79	Cock et al.[55]	https://github.com/biopython/biopython/blob/master/README.rst
Inkscape Version 1.2	2021 Inkscape Developers	https://inkscape.org/
AlphaFold 2	DeepMind and EMBL-EBI	https://alphafold.com/
Jalview	Waterhouse et al.[56]	https://www.jalview.org/

(*Continued on next page*)

Continued

REAGENT or RESOURCE	SOURCE	IDENTIFIER
Phyre2	Kelley et al.[57]	http://www.sbg.bio.ic.ac.uk/phyre2
PyMOL Molecular Graphics System version 2.0	Schrödinger, LLC	https://pymol.org/2/
Other		
PacBio Sequencing	Sequel IIe System	https://www.liverpool.ac.uk/genomic-research/technologies/next-generation-sequencing/
Nanopore Sequencing	Source Genomics	https://sourcebioscience.com/genomics/nanopore-sequencing/
Sanger Sequencing	Source Genomics	https://sourcebioscience.com/genomics/sanger-sequencing/
Sanger Sequencing	Eurofins Genomics	https://eurofinsgenomics.eu/en/custom-dna-sequencing/

RESOURCE AVAILABILITY

Lead contact

Further information and requests for resources and reagents should be directed to and will be fulfilled by the lead contact, Anne Chevallereau (anne.chevallereau@cnrs.fr).

Materials availability

All unique phages, bacteria, and plasmids used in this study are available from the lead contact without restrictions.

Data and code availability

Sequencing data have been deposited in NCBI under the BioProject accession number PRJEB61545. Ordinary differential equations generated for mathematical modelling are included in STAR Methods. Bacterial and archaeal RefSeq assemblies and scripts used to carry out bioinformatic analyses are available at https://github.com/elliekpursey/Maestri. Source data for Figures 1, 3, 4, 5, S1, and S2 are available at https://github.com/alicemaestri/raw_data_MADS_CHM.

EXPERIMENTAL MODEL AND SUBJECT DETAILS

Bacterial strains

P. aeruginosa UCBPP-PA14 *csy3::lacZ*[43] (referred to as PA14ΔCRISPR, since it carries a disruption of an essential *cas* gene that causes the CRISPR-Cas system to be non-functional), was grown overnight at 28°C or 37°C in LB broth. *P. aeruginosa* SMC4386[26] (referred to as SMC4386-WT), and deletion mutants of this strain (referred to as ΔCRISPR, ΔMADS, ΔCRISPRΔMADS, Δ*mad1*, Δ*madi2*, Δ*mad3*, Δ*mad4*, Δ*mad6*, Δ*mad7*, Δ*mad8*) were growth at 28°C or 37°C in either LB broth or M9 medium (22 mM Na_2HPO_4; 22 mM KH_2PO_4; 8.6 mM NaCl; 20 mM NH_4Cl; 1 mM $MgSO_4$; 0.1 mM $CaCl_2$) supplemented with 0.2% glucose. *P. aeruginosa* PAO1[44] was grown overnight at 37°C in LB broth and was used for phage amplification, *Escherichia coli* MFD*pir*[46] was used as donor to build the transposon mutant library; *E. coli* DH5α (Thermo Fisher Scientific) was used to assemble the allelic exchange vectors for the gene deletions, to assemble the pLola plasmids, and to perform site directed mutagenesis; *E. coli* S17-1λ*pir*[47] was used as donor strain to deliver the allelic exchange vectors to recipient cells during conjugation assays; *E.coli* MG1655[45] was used as source for the Rhamnose promoter subsequently cloned into the pLola plasmids. Whenever applicable, media was supplemented with ampicillin (100 μg/mL), streptomycin (50 μg/mL), or gentamicin (either 30 μg/mL or 20 μg/mL, when selecting for *E. coli*, or 50 μg/mL, when selecting for *P. aeruginosa*) to ensure plasmid maintenance. *E. coli* MFD*pir*[46] was cultured in the presence of diaminopimelic acid (DAP) (0.3 mM).

Phage strains

Phages used in this study are listed in the key resources table. Recombinant temperate phage DMS3-Gm,[24] which encodes a gentamycin resistance gene, was used to enable selection of lysogens following infection of WT and mutant SMC4386 strains as well as the transposon mutant library. Phage DMS3*vir*,[43] which is obligately lytic due to the deletion of the c-repressor gene, and/or phage DMS3*vir*Δ*acrIE3*,[48] which lacks both the c-repressor gene and the anti-CRISPR gene that blocks the Type IE CRISPR-Cas system of strain SMC4386, were used in all other experiments, and have been described previously.[43,48] Phages PA14P2,[49,50] JBD25[43] and LPB1 were used in spot assays to determine the range of resistance conferred by MADS. Phage stocks were extracted from lysates prepared on *P. aeruginosa* PA14ΔCRISPR, PAO1 or SMC4386ΔCRISPR and stored at 4°C.

METHOD DETAILS

Adsorption assay

The measurement of phage adsorption was performed according to Kropinsky, 2009[58] with some modifications. Briefly, 9 mL of *P. aeruginosa* SMC4386-WT and PA14ΔCRISPR culture (OD_{600}=0.25) were infected with $2x10^6$ plaque forming units (PFU)/mL of phage DMS3*vir*. Every 6 min for 1h, an aliquot of 100 μL was taken from each vial and transferred into a chilled Eppendorf tube containing 800 μL of LB broth and 100 μL of chloroform. Extracted phages were serially diluted and spotted onto a lawn of *P. aeruginosa* PA14ΔCRISPR to determine the phage titer. The experiment was carried out in a water bath, at 28C and with 100 rounds per minute (rpm) agitation.

Efficiency of Plaquing (EOP) assays

EOP assays were carried out on square polystyrene plates containing LB with 1.5% agar. A mixture of molten soft LB agar (0.5%) and 300 μL of bacteria (grown overnight in LB broth) were poured on top of the hard agar layer and allowed to set. Next, 5 μL of serially diluted phage were spotted on the resulting plates, which were subsequently incubated overnight at 28ºC and plaque forming units (PFUs) were enumerated the next day. The EOP was determined as the ratio of the number of PFUs on a mutant *P. aeruginosa* SMC4386 and the *P. aeruginosa* SMC4386-WT or SMC4386ΔCRISPR strains. To be able to calculate the EOP with DMS3*virΔacr*, we arbitrarily set the phage titer on *P. aeruginosa* SMC4386-WT at 1 PFU/mL (instead of 0).

Generation of the transposon (Tn)-mutant library

To generate the transposon-mutant library we used the synthetic construct pBAM (born-again-mini-transposon) described by Martínez-García et al.[59] Specifically, we utilized the vector pBAMD1-4,[51] which delivers the Tn5 while conferring resistance to streptomycin to the target cells at the same time, allowing for selection of transconjugants. The pBAMD1-4 vector was delivered to the recipient bacteria via conjugation using the *E. coli* MFD*pir* strain as donor cell, following previously described methods.[46] Briefly, we separately incubated 15 mL of *E. coli* MFD*pir* donor cells and recipients (*P. aeruginosa* SMC4386-WT and SMC4386ΔCRISPR strains), which were incubated overnight at 37C with agitation at 180 rpm. Recipients were grown in LB broth, while donors were grown in LB broth supplemented with DAP (0.3mM), ampicillin (100 μg/mL) and streptomycin (50 μg/mL). The following day, 10 mL of each strain was pelleted and washed twice with 10 mL of M9 salts saline solution. Bacterial cultures where pelleted again and resuspended in 10 mL of LB supplemented with 0.3 mM DAP. Donors and recipient were mixed together (7500 μL donor: 500 μL recipient), pelleted and resuspended in 1 mL of M9 saline solution. To allow for conjugation between donor and recipient, 100 μL of mix was spotted onto 10 individual Binder-Free Glass Microfiber 1.2 μM filter papers (Whatman) which were placed onto a squared LB agar plate supplemented with DAP (0.3 mM), and incubated at 28C for 48h. Cells from each filter were then recovered into LB supplemented with streptomycin (to kill the non-transconjugants), pelleted, washed twice (resuspended first in 1 mL and then in 100 μL) and plated onto an LB agar plate supplemented with streptomycin to select for the transconjugants. Plates were incubated for 24-48h at 28C. For each recipient strain, an *E. coli* MFD*pir* donor strain without plasmid was used as negative control. Based on pilot data that yielded around 1000 transconjugants, this procedure was carried out in 10 independent biological replicates, which were pooled during the last step in order to obtain a saturated Tn mutant library.

Measuring frequencies of lysogeny

Lysogeny in PA14ΔCRISPR, SMC4386 and derivative knockouts strains

Cultures were grown overnight at 37C with 180 rpm agitation, in 6 mL of LB broth. Cultures were then diluted 1:100 into fresh LB broth and infected with phage DMS3-Gm[24] at an MOI of 0.01. After 24h, samples were serially diluted, plated onto selective (LBA with Gm) and non-selective (LBA) agar plates and incubated overnight at 28C. Colonies were enumerated the next day. The proportion of lysogens was expressed as the number of CFU (Colony Forming Units) grown on selective plates divided by the number of CFU on non-selective media.

Lysogeny in the Tn5 mutants library

The transconjugants (see generation of the transposon (Tn)-mutant library for details on how they were obtained) were scraped off LBA plates, pooled, and resuspended in 10 mL of LB broth and then infected with 10^5 PFU of phage DMS3-Gm, followed by overnight incubation at 28C with agitation at 180 rpm.

Each day and for 3 days, 1 mL of the culture was transferred into 10 mL of fresh LB broth, the phages were extracted to monitor phage titer and bacteria were plated onto non-selective LBA as well as LBA supplemented with streptomycin (selecting for Tn mutants) or both streptomycin and gentamicin (selecting for Tn mutants carrying the DMS3-Gm prophage). Plates were incubated at 28C for 24-48h. Lysogenization of bacterial colonies on LBA with streptomycin and gentamicin was confirmed by colony PCR using primers Crep_F (forward, 5'- GCGGAATGAGCGCTAAACC-3') and Crep_R (reverse, 5'- CAAGTGCTTTAGCGAGGAATGC-3'), that amplify the c-repressor gene of phage DMS3.

Localization of the Tn5 insertions

Before being subjected to arbitrary PCR (described below), we verified using colony PCR that the clones of interest carried the miniTn5 insertion using the primer pairs PS5 (5'-CCCTGCTTCGGGGTCATT-3') and PS4 (5'-CCAGCCTCGCAGAGCAGG-3'), and PS5 and PS6 (5'-GGACAAATCCGCCGCCCT-3'), using cells carrying the plasmid pBAMD1-4 as a positive control. Both primer pairs

amplify the *oriT* region of the plasmid, leading to a product size of 225 bp and 665 bp respectively. Only in case of absence of *oriT* amplification we proceeded with the arbitrary PCR. Next, we applied a protocol of arbitrary PCR to identify the location of Tn5 insertions, based on the methods described by Martínez-García et al.[51] and Saavedra et al.[60] In the first round of arbitrary PCR we used the forward primer ME-O-Sm-Ext-F (5'- CTTGGCCTCGCGCGCAGATCAG-3') and the reverse primer ARB6 (5'- GGCACGCGT CGACTAGTACNNNNNNNNNNACGCC-3'), while in the second round of arbitrary PCR we used the forward primer ME-O-Sm-Int-F (5'- CACCAAGGTAGTCGGCAAAT-3') and the reverse primer ARB2 (5'-GGCACGCGTCGACTAGTAC-3'). We followed the PCR conditions that have been previously described.[51] Since all the transconjugants are different from one another (i.e., the Tn5 is in different location in the bacterial genome), some PCR conditions, such as the annealing temperature, work for some clones but not for others. Therefore, for clones where we did not obtain clear and definite bands after the second round, we adjusted the protocol as follows: in the first round the number of cycles increased from 30 to 35 and/or the annealing temperature gradually increased to a maximum of 38℃; in the second round the annealing temperature increased to 52℃. PCR products obtained after the second round of arbitrary PCR were gel purified and sent for Sanger sequencing (Eurofins Genomics UK Limited, Wolverhampton, UK). The chromatogram derived from the Sanger sequencing was mapped against the genome of *P. aeruginosa* SMC4386-WT using Geneious v10.2.6 to identify the genes where the transposon was inserted.

Generation of gene knockouts

The deletion of CRISPR-Cas and MADS systems, as well as the deletion of single genes from MADS were carried out using two-step allelic exchange, as described by Hmelo et al.[52] The homologous sequences flanking either side of the desired target system and/or gene were synthesized by Integrated DNA Technology (IDT00E4) or PCR amplified and fused together via SOE-PCR,[61,62] and then cloned into the pDONRPEX18Gm donor vector via Gateway cloning. The resulting allelic exchange vector was transformed into chemically competent *E. coli* DH5α and verified by PCR. Vectors were then electroporated into competent *E.coli* S17-1λ*pir* to allow for conjugation with *P. aeruginosa* SMC4386-WT recipient strains.[52] The merodiploids that were obtained were selected on cetrimide agar plates (to select for *P. aeruginosa*) supplemented with gentamicin (50 μg/mL). Every genomic deletion was confirmed by colony PCR, first by positive amplification of the knockout junction, and then by negative amplification of the left and right side of the intact system and/or gene, followed by Sanger sequencing (Eurofins Genomics UK Limited, Wolverhampton, UK). The list of primers used to generate and screen the knockout strains are listed in Table S6.

Growth curves

Growth curves to assess the role of MADS during infection with phage DMS3*vir* were performed in 96-well plates with agitation at 37℃. Briefly, overnight cultures of WT and mutant strains of *P. aeruginosa* SMC4386 grown in LB media at 37℃ with agitation at 180 rpm were diluted 100-fold into fresh LB media and grown until cultures reached mid-log phase (OD600 nm of 0.3, approximately 10^8 CFU/mL). One mL of each mid-log culture was centrifuged for 3 min at 6000 rpm to remove the supernatant and the pellets were infected with 1 mL of DMS3*vir* at an MOI of 10 in LB and incubated for 10 min at 37℃ whilst shaking at 180 rpm. After initial incubation to synchronize the infection, 200 μL of the infected cultures were transferred to a 96-well plate, then 20 μL of mineral oil were added on the surface of each well to avoid evaporation and bacterial growth was measured by optical density at 600 nm (OD600) for 24h at 37°C with agitation in a BioTek Synergy 2 plate reader. At t=0 200μL samples were used to quantify initial bacteria CFU/mL and phage titre PFU/mL. Growth measurements in the absence of phage were carried out in parallel as a control.

Construction of pLola plasmids

To express individual genes from MADS operon in *P. aeruginosa* a shuttle vector for *E. coli* and *P. aeruginosa* pLoLa was assembled according to SEVA (Standard European Vector Architecture) guidelines (Home - SEVA plasmids - Standard European Vector Architecture (seva-plasmids.com)). The genes of interest (*mad1*, *mad2*, *mad3*, *mad4*, *mad6 and mad7*) and promoter region of MADS operon (MADSP) were synthesized by Twist Bioscience (San Francisco, CA, USA). Rhamnose promoter (RhaP) sequence and auxiliary genes were amplified by PCR from the genome DNA of *E. coli* MG1655 strain. PCR amplification of each fragment was performed using primers with overlaps complementary to adjacent parts for assembly (see Table S7). The vector backbone was amplified to include compatible overhangs for the inserts (see Table S7). Recombinant plasmids were assembled using HiFi NEBuilder Assembly Kit (New England Biolabs) according to the manufacturer's instructions. The resulting plasmids carried one of the *mad* genes (or sequence of *mCherry* gene for negative control) under the control of either RhaP or MADSP (see key resources table for the complete plasmids list). Chemically competent *E. coli* DH5α cells were transformed with the resulting plasmids, which were then verified by PCR to confirm the presence and correct orientation of the inserts (see Table S6), followed by Nanopore sequencing (Source BioScience, Nottingham, UK) for in-depth verification.

Complementation assay

The pLola plasmids carrying the desired *mad* gene and the desired promoter (rhamnose or native), as well as a control plasmid carrying a *mCherry* gene instead of the *mad* gene, were transformed in *P. aeruginosa* isogenic ΔCRISPRΔ*mad1*, ΔCRISPRΔ*mad2*, ΔCRISPRΔ*mad3*, ΔCRISPRΔ*mad4*, ΔCRISPRΔ*mad6*, or ΔCRISPRΔ*mad7* (e.g., the pLola-*mad1*-RhaP and the control pLola-*mCherry*-RhaP were transformed into the *P. aeruginosa* ΔCRISPRΔ*mad1* strain).

Plasmid transformation was confirmed by colony PCR using primers pLola_ins_seq_for (5'-AGATGGAGTTCTGAGGTCAT TACTGG-3') and AO_R24 (5'-AGCGGATAACAATTTCACACAGGA-3') that amplify the *mad* or the *mCherry* genes.

Next, we performed a spot test of phage DMS3*vir* serially diluted onto lawns of *P. aeruginosa* ΔCRISPR and lawns of isogenic ΔCRISPRΔ*mad1*, ΔCRISPRΔ*mad2*, ΔCRISPRΔ*mad3*, ΔCRISPRΔ*mad4*, ΔCRISPRΔ*mad6* or ΔCRISPRΔ*mad7* transformed with the pLola plasmid carrying the missing *mad* gene. As a control, a spot test onto lawns of each of the isogenic ΔCRISPRΔ*mad genes* strains, either non-transformed with any plasmid, or transformed with the control plasmid pLola carrying the *mCherry* gene was performed in parallel.

The pLola plasmids carrying *mad1*, *mad2*, *mad3* and *mad7* were under the control of the inducible rhamnose promoter, whereas *mad4* and *mad6* were under the control of the MADS native promoter. Consistently, during complementation of ΔCRISPRΔ*mad1*, ΔCRISPRΔ*mad2*, ΔCRISPRΔ*mad3* and ΔCRISPRΔ*mad7* we transformed each isogenic strain with the control plasmid pLola-*mCherry*-RhaP, while during complementation of ΔCRISPRΔ*mad4* and ΔCRISPRΔ*mad6* we transformed the isogenic strains with the control plasmid pLola-*mCherry*-MADP. We used the native promoter, instead of the inducible rhamnose promoter for the complementation of *mad4* and *mad6* because expression of those genes from the rhamnose promoter lead to cell toxicity (the bacterial lawn did not grow), presumably due to overexpression. To ensure the expression of the genes under the control of the rhamnose promoter, the spot test was performed using LB agar plates supplemented with rhamnose 0.2%. Gentamicin (50 μg/mL) was added to overnight cultures and to LB agar plates to ensure plasmid maintenance. The EOP was calculated relative to the *P. aeruginosa* ΔCRISPR strain.

Bioinformatic analysis of the distribution of MADS

Analysis of protein domains and HMM profiles

MADS locus protein sequences were determined from genome annotations made using Prokka v1.14.6, which uses Prodigal to predict protein regions. These proteins were searched against the pfam (protein family) database, as well as Phyre2 and HHpred, to perform HMM-HMM matching-based remote homology detection and obtain structural predictions.[63,57] Curated alignments for each gene were constructed by identifying homologues for each protein sequence using HHpred. A probability cut-off score of 50% was set, with default parameters for all other options, searching against the PDB database. Alignments extracted from HHpred outputs (max 250 sequences) were then used to generate profile-HMMs using the *hmmbuild* function from HMMER v3.0. For further investigations of remote homology, HHpred was run against the PDB, COG, NCBI conserved domains and Pfam-A databases.

Genomes

A total of 172,366 bacterial and archaeal RefSeq assemblies (retrieved January 2022 using ncbi-genome-download, https://github.com/kblin/ncbi-genome-download/) were downloaded for use in prevalence analysis. To further characterise defense islands in *P. aeruginosa*, a total of 454 publicly available complete genomes were obtained from GenBank.

Macromolecular models for MADS

MacSyFinder v2, a tool for macromolecular systems detection,[30] was used to develop models for MADS. This tool requires the specification of mandatory or accessory components within the system, which are not biological definitions but rather describe whether a protein is easy to detect or more divergent and thus harder to detect with a single HMM profile, as well as whether components are frequently missing from systems.

After making sure that no known anti-phage systems could be identified by PADLOC[27] and DefenseFinder[28] within the MADS operon (Table S1), genomes were retrieved in genbank (.gbff) format and ordered protein fasta files were created by extracting the CDS features using SeqIO from Biopython.[55] Initial models with various levels of system completeness and genomic distance between components were tested. Initially, all *P. aeruginosa* RefSeq genomes (n=6,103) were searched. Next, preliminary tests, and manual inspection of hits from a subset of the entire Bacterial and Archaeal RefSeq dataset (n=15,000), the following model parameters were set. Proteins MAD6, 7 and 8 were defined as mandatory and their presence was required for the system to be detected. Proteins MAD1, 2 and 5 were defined as accessory due to their homology to Restriction-Modification system components and widespread regulators, which could lead to false positive hits if made mandatory. Finally, proteins MAD3 and 4 were also classified as accessory, due to them not being reliably detected in all systems. In addition, the maximum inter gene distance was set to 10.

Taxonomic distribution and plots

Species classifications for genomes with MADS were retrieved using the Entrez python module. Taxonomic trees were retrieved from NCBI using the ete3 v3.1.2 module, and used to visualize the phylogenetic distribution of MADS. Other plots were created in R, with operons plotted using gggenes. Additional editing of plots was performed using Inkscape v1.2.

Reproducibility and computational resources

The University of Exeter's Advanced Research Computing Facilities were used to carry out for this bioinformatics analysis. A Snakemake pipeline was used to run MacSyFinder searches on all genomes, whilst the remaining analyses were carried out using R v4.0.4 and Python version 3.9.7 with Biopython v1.79. All scripts used for this analysis are available at https://github.com/elliekpursey/Maestri.

Frequency of MADS and CRISPR-Cas and their co-occurrence

The output from running PADLOC[27] on a total of 233,092 genomes in the RefSeq database (v209) (data kindly provided by Dr. Simon Jackson in November 2023) was used to measure the frequency and co-occurrence of MADS and CRISPR-Cas defense systems. The total numbers of MADS, all CRISPR-Cas and Cas-Type-I-E and I-F systems were calculated from the PADLOC[15] output and all corresponding genome accession numbers were extracted. Custom python scripts utilising the BioPython v1.79 library, Entrezpy (https://academic.oup.com/bioinformatics/article/35/21/4511/5488119), were used to obtain species and kingdom information

from the Entrez database at National Center for Biotechnology Information (NCBI). The presence of defense systems of interest was then stratified by species and used to calculate co-occurrence.

Bioinformatic analysis of defense islands

A total of 445 publicly available complete *P. aeruginosa* genomes were included in the assessment of the putative defense island (Table S4). Defense islands were extracted from genomes by first examining the BLASTx percentage identity and genome coordinates against relevant query reference sequences of the distinct gene boundaries pheT (MPAO1_RS11510) and a histidine kinase (MPAO1_RS11445).[64] FASTA sequence files of defense islands were extracted from complete genome FASTA files using BEDTools v2.29.2 getfasta and subtract, based upon BLASTx genome coordinates.[54] Prokka v1.14.6 was used to annotate defence islands and the remainder of the genome.[53] Defense systems in all sequence files were identified using PADLOC[27] and DefenseFinder,[28] both with additional CRISPR array detection. Wilcoxon's signed rank testing was used to determine enrichment for defense systems on the island and was performed using R v4.1.3. Manual inspection of the defense hotspots containing MADS was carried out using Geneious v10.2.6

Analysis of MADS self/non-self discrimination

Infection assays in liquid medium

Infection assays to measure the population dynamics of phage DMS3*vir* in the presence or absence of MADS were performed in glass vials by inoculating 6 mL M9 medium supplemented with 0.2% glucose with approximately 5 x 10^7 CFU bacteria from fresh overnight cultures (also grown in M9 medium + 0.2% glucose) of either *P. aeruginosa* SMC4386-WT strain or the isogenic ΔCRISPR, ΔMADS or ΔCRISPRΔMADS strains. Cultures were infected at MOI 0.1 and 10, incubated at 37℃ while shaking at 180 rpm and transferred daily (1:100 dilution) for three days into fresh medium. Phages were chloroform extracted (1:10 volume) every day and their titers measured via spot test assay onto a lawn of the sensitive *P. aeruginosa* PA14ΔCRISPR strain. Plates were incubated overnight at 28℃. We monitored whether phages in these experiments evolved to overcome bacterial defense systems, and whether this was due to genetic or epigenetic mutations. To this end, we performed plaque-purification of phages from the SMC4386 lawns using chloroform extractions, and phage were titrated on lawns of SMC4386-WT and PA14ΔCRISPR strains. These phages were then used in a next round of parallel infections on SMC4386-WT or PA14ΔCRISPR strains as hosts, at 28℃ in glass vials containing 6mL of LB broth, while shaking at 180 rpm. Phages were chloroform extracted again, and titrated on both strains. This process was repeated for another round of infection, to understand the heritability of the escape phenotype of the phage.

Phage and bacteria DNA extraction for sequencing

For phage DNA extraction the 4 replicate experiments of DMS3*vir* that during infection assays with *P. aeruginosa* SMC4386ΔCRISPR (referred to as ΔCRISPR) gained the capability to amplify after 2 days of infection (see Figure 4A), were amplified on ΔCRISPR and ΔCRISPRΔ*mad2*, which is the mutant lacking the predicted methyltransferase, while the ancestral DMS3*vir* was amplified on ΔCRISPRΔMADS. To this end, 500 μL of bacteria from a fresh overnight culture were inoculated into 50 mL of LB broth and mixed with 100 μL of an approximately 1x10^8 PFU phage stock. Those infected cultures were grown overnight in 50 mL of broth at 28℃, 180 rpm. The resulting viscous cultures were centrifuged at 25,000 x*g* and phages were found to have concentrated in the pellet. The pellet was resuspended with 5 mL of phosphate buffered saline (PBS) and centrifuged at 21,000 x*g* to remove bacterial cells. Phages were concentrated from the supernatant using 0.5 mL 100kDa Amicon spin filters as per the manufacturer's guidelines and retained in the filters. Whilst still in the filter, phages were washed twice with DNase I buffer (up to 400 μL), treated with DNase I as per the manufacturer's guidelines, washed twice with RNase buffer (up to 400 μL), treated with RNase A as per the manufacturer's guidelines, washed twice with RNase buffer (up to 400 μL) and eluted from the Amicon filters by inversion and centrifugation with RNase buffer (up to 400 μL) to give a final volume for each phage solution of 400 μL. Phage DNA was extracted using a proteinase K lysis step (20 μg of proteinase K, 0.5% SDS, 20mM EDTA pH 8.0) for 1 h at 60 ℃ followed by 2 phenol:chloroform extractions (1:1 volume, inversion and centrifugation), DNA was precipitated using sodium acetate (1/10 volume, 3M, pH 7.5 and ethanol (2.5 volume, 100%, ice-cold) overnight at -20℃. DNA was pelleted (30min, 20,000 x*g*, 4℃) and washed twice with ice-cold 70% ethanol, dried and resuspended in TE buffer.

For bacterial DNA extraction (*P. aeruginosa* SMC4386-WT, SMC4386ΔCRISPR, SMC4386ΔCRISPRΔMADS, SMC4386ΔCRISPRΔ*mad2*) bacteria were pelleted from overnight culture and DNA was extracted using the phenol chloroform method outlined previously. Quality Control and quantification of bacteria and phage DNA was performed with NanoDrop, Qubit and agarose gel electrophoresis; 2 μg of DNA were used for Pacific Biosciences (PacBio) sequencing (Centre For Genomic Research, Liverpool, UK).

PacBio sequencing

Barcoded SMRT-Bell PacBio libraries were created from each DNA sample and run on a SMRT cell in CLR mode on a Sequel IIe platform, yielding >300,000x coverage for phage samples and 1,400 – 2,200x coverage for bacterial samples. The PacBio SMRT-Link v10.0 analysis pipeline (https://www.pacb.com/support/software-downloads/) was used to demultiplex samples, to detect methylation signals based on polymerase kinetics, and to identify motifs associated with methylation, all under default parameters. Resulting diagnostic plots and gff files were inspected manually. Output files, including logs, are available at https://github.com/scottishwormboy/Maestri_pbio. The genome reference used for DMS3 was NC_008717.1. For SMC4386, the PacBio reads were used to create a new genome reference (accession: GCF_026636135.1) from the wild-type, using SMRT-Link v10.0 for microbial assembly.

CRISPR immunosuppression assay

CRISPR immunosuppression assays were performed as previously described.[62,65] This assay relies on transformation of *P. aeruginosa* SMC4386 cells with plasmid pHERD30T[20] (non-targeted by the SMC4386 CRISPR-Cas system) and pHERD30T-cr1sp2-SMC (targeted by SMC4386 CRISPR-Cas system). Briefly, the pHERD30T-cr1sp2-SMC plasmid was constructed by inserting a 32 nucleotide protospacer matching the 2nd spacer of CRISPR array 1 of the *P. aeruginosa* SMC4386 strain, flanked by the AAG Protospacer Adjacent Motif (PAM). Oligonucleotides containing the PAM and protospacer sequence (5'-agcttAAGAACCTCTAC GAGCAGACCGAGTTGAAAGGGCAg-3' and 5'- aattcTGCCCTTTCAACTCGGTCTGCTCGTAGAGGTTCTTa-3', restriction sites overhangs are indicated in small caps, protospacer in capitals and PAM underlined) were annealed to create overhangs compatible with HindIII and EcoRI, phosphorylated by T4 Polynucleotide Kinase and ligated in EcoRI-HindIII digested pHERD30T vector. Cultures of *P. aeruginosa* SMC4386-WT and isogenic ΔCRISPR, ΔMADS and ΔCRISPRΔMADS strains grown overnight in 50 mL of LB medium (approximately 3.5 x 10^9 CFU/mL) were divided in three 50 mL tubes with 10 mL of culture in each. Cells were either non-infected or infected using a final density of 10^9 PFU/mL (MOI=0.3) of DMS3*vir* or DMS3*vir*Δ*acrIE3*. After 2h of incubation at 37C with agitation at 180 rpm, cells were harvested by centrifugation at 3500 rpm for 15 minutes. A sample of the supernatant was kept for phage titration by spot assay to validate homogeneity of the phage titre across the replicates. Cells were made electrocompetent by washing them twice with 1 mL of 300 mM sucrose solution at room temperature and resuspended in 300 μL of the same solution. A 100 μL sample of the resuspended cells was taken to evaluate the bacterial density. The remaining 200 μL were equally divided across two vials and electroporated with 500 ng of either pHERD30T or pHERD30T- cr1sp2-SMC, followed by addition of 700 μL fresh LB medium. After incubating for 1h at 37C at 180 rpm, bacteria were pelleted, resuspended in 100 μL of LB medium and serially diluted in LB-medium. Fifty microliters of each dilution were spotted on LB agar plates containing gentamycin (50 μg/mL) and incubated overnight at 37C to allow transformants to grow. Relative transformation efficiency was calculated as the number of colonies obtained after transformation with pHERD30T- cr1sp2-SMC divided by the number of colonies obtained after transformation with pHERD30T.

Plasmid transformation assays – Methylation pattern

This assay was adapted from the CRISPR immunosuppression assay to fit the MADS. It relies on transformation of *P. aeruginosa* SMC4386 cells with plasmid pHERD30T[20] (non-targeted by the SMC4386 MADS) and pHERD30T-M24 (targeted by SMC4386 MADS). Briefly, the pHERD30T-M24 plasmid was constructed by inserting an 11 nucleotide MADS target sequence (5'-TCAGCGCG TCC-3'). Oligonucleotides containing the target sequence (5'-agcttTCAGCGCGTCCg-3' and 5'-aattcGGACGCGCTGAa-3', restriction sites overhangs are indicated in small caps and target sequence in capitals) were annealed to create overhangs compatible with HindIII and EcoRI, phosphorylated by T4 Polynucleotide Kinase and ligated in EcoRI-HindIII digested pHERD30T vector. This plasmid, as well as a non-targeted pHERD30T control plasmid, were then transformed in *P. aeruginosa* SMC4386ΔCRISPRΔMADS or isogenic ΔCRISPRΔ*mad1*, ΔCRISPRΔ*mad2*, ΔCRISPRΔ*mad3*, ΔCRISPRΔ*mad4*, ΔCRISPRΔ*mad6*, ΔCRISPRΔ*mad7*, ΔCRISPR Δ*mad8*, ΔCRISPRΔ*mad2*Δ*mad5* or ΔCRISPRΔ*mad3*Δ*mad5*. These transformed strains were then used for plasmid production, which were purified with GeneJET Plasmid Midiprep kit (Thermo Scientific, USA) according to the manufacturer's instructions.

Cultures of *P. aeruginosa* SMC4386-ΔCRISPR and ΔCRISPRΔMADS strains grown overnight in 100 mL of LB medium (approximately 3.5 x 10^9 CFU/mL) were harvested by centrifugation at 3500 rpm for 15 minutes. Cells were made electrocompetent by washing them twice with 10 mL of 300 mM sucrose solution at room temperature and resuspended in 2 mL of the same solution. SMC4386 -ΔCRISPR and ΔCRISPRΔMADS cell suspensions were equally divided across twenty vials each, were electroporated with 500 ng of pHERD30T and pHERD30T-M24 produced in each SMC4386 deletion strain, followed by addition of 700 μL fresh LB medium. After incubating for 1h at 37C at 180 rpm, bacteria were pelleted, resuspended in 100 μL of LB medium and serially diluted in LB-medium. Forty microliters of each dilution were spotted on LB agar plates containing gentamycin (50 μg/mL) and incubated overnight at 37C to allow transformants to grow. Relative transformation efficiency was calculated as the number of colonies obtained after transformation with pHERD30T-M24 divided by the number of colonies obtained after transformation with pHERD30T-Nonmeth, the two plasmids being produced in the same strain.

Plasmid *in vitro* digestion assay

The pHERD30T-MADS-EcoRI plasmid was constructed by inserting a 11 nucleotide MADS target sequence overlapping with an EcoRI target sequence (5'- TCAGGAATTCC-3', EcoRI sequence underline). Oligonucleotides containing the target sequence (5'-agcttTCAGGAATTCCc-3' and 5'-catggAGTCCTTAAGGa-3', restriction sites overhangs are indicated in small caps and target sequence in capitals) were annealed to create overhangs compatible with HindIII and NcoI, phosphorylated by T4 Polynucleotide Kinase and ligated in EcoRI-NcoI digested pHERD30T vector. This plasmid, as well as a non-targeted pHERD30T control plasmid, were then transformed in *P. aeruginosa* SMC4386ΔCRISPRΔMADS or isogenic ΔCRISPRΔ*mad1*, ΔCRISPRΔ*mad2*, ΔCRISPRΔ *mad3*, ΔCRISPRΔ*mad4*, ΔCRISPRΔ*mad6*, ΔCRISPRΔ*mad7*, ΔCRISPRΔ*mad8*, ΔCRISPRΔ*mad5*Δ*mad2* or ΔCRISPRΔ*mad5*Δ *mad3*. These transformed strains were then used for plasmid production, which were purified with GeneJET Plasmid Midiprep kit (Thermo Scientific, USA) according to the manufacturer's instructions.

The produced plasmids were then double-digested with NheI-HF (NEB, USA), to linearize the plasmid, and EcoRI-HF (NEB, USA), to test for methylation presence. The digestion was performed according to the manufacturer's instructions, with a 1h incubation at 37C. Reaction was stopped by adding TriTrack DNA loading dye (Thermo Scientific, USA) according to the manufacturer's

instructions, and digestion mixes were loaded on a 1% agarose gel (migration 40 min at 100 V). Gel were imaged with a GelDoc Imaging System (BioRad, USA) and band quantification was done with the Image Lab software (BioRad, USA).

Plasmid transformation assays – Restriction pattern

For the restriction pattern experiments, plasmids were produced in *P. aeruginosa* SMC4386 ΔCRISPRΔMADS (called pHERD30T-Nonmeth and pHERD30T-M24-Nonmeth) and ΔCRISPRΔmad1 (called pHERD30T-Meth and pHERD30T-M24-Meth).

Cultures of *P. aeruginosa* SMC4386 WT, ΔCRISPR, ΔMADS, ΔCRISPRΔMADS, ΔCRISPRΔ*mad1*, ΔCRISPRΔ*mad2*, ΔCRISPRΔ*mad3*, ΔCRISPRΔ*mad4*, ΔCRISPRΔ*mad6*, ΔCRISPRΔ*mad7*, ΔCRISPRΔ*mad8*, ΔCRISPRΔ*mad5*Δ*mad2* or ΔCRISPRΔ*mad5*Δ*mad3* strains grown overnight in 20 mL of LB medium (approximately 3.5 x 10^9 CFU/mL) were harvested by centrifugation at 3500 rpm for 15 minutes. Cells were made electrocompetent by washing them twice with 2 mL of 300 mM sucrose solution at room temperature and resuspended in 400 μL of the same solution. Each cell suspension was equally divided across four vials and electroporated with 500 ng of either pHERD30T-Nonmeth, pHERD30T-M24-Nonmeth, pHERD30T-Meth or pHERD30T-M24-Meth, followed by addition of 700 μL fresh LB medium. After incubating for 37°C at 180 rpm, bacteria were pelleted, resuspended in 100 μL of LB medium and serially diluted in LB-medium. Forty microliters of each dilution were spotted on LB agar plates containing gentamycin (50 μg/mL) and incubated overnight at 37°C to allow transformants to grow. Relative transformation efficiency of methylated or non-methylated plasmids (respectively) were calculated as the number of colonies obtained after transformation with pHERD30T-M24-Nonmeth or pHERD30T-M24-Meth divided by the number of colonies obtained after transformation with pHERD30T-Nonmeth or pHERD30T-Meth, respectively.

Phenotypic interactions between CRISPR-Cas and MADS

Tipping-point assay

Infection assays were performed in glass vials by inoculating 6 mL M9 medium supplemented with 0.2% glucose with approximately 10^7 CFU bacteria from fresh overnight cultures (also grown in M9 medium + 0.2% glucose) of the *P. aeruginosa* SMC4386-WT strain and the isogenic ΔCRISPR, ΔMADS and ΔCRISPRΔMADS strains. To these vials, phage DMS3*vir* was added at a MOI of 10^{-4}, 10^{-3}, 10^{-2}, 10^{-1}, 1, 10^1, or 10^2, and incubated at 37°C while shaking at 180 rpm. Cultures were transferred daily (1:100 dilution) for three days into fresh M9 medium. Phages were chloroform extracted every day and the titers were measured using spot assays onto lawns of each of the four different bacterial strains (i.e., *P. aeruginosa* SMC4386-WT, ΔCRISPR, ΔMADS and ΔCRISPRΔMADS strains). Plates were incubated overnight at 28°C.

To identify replicate experiments in which phage mutants had emerged that escape MADS, we determined for each phage sample the EOP ratio's on *P. aeruginosa* SMC4386ΔCRISPRΔMADS and either the ΔCRISPR or WT bacteria. For WT DMS3*vir* phages, these ratios are 127 ±17 and 142 ± 33 (mean ± 95% c.i.), respectively. For clonal phage populations of DMS3*vir* escape mutants (carrying the epigenetic modification to overcome MADS), these ratios are 0.91 ± 0.15 and 1.18 ± 0.12 (mean ± 95% c.i.), respectively. We therefore applied a conservative threshold of EOP=5 (i.e. corresponding to ± 20% escape mutants in the phage population) to identify samples that contained significant numbers of MADS escape phages. Replicates where escape phages were detected are depicted as red circles in Figures 4D and 4E.

Invasion assay – mixed infections with phages DMS3vir-WT and DMS3vir-methylated

Infection assays were performed in glass vials by inoculating 6 mL M9 medium supplemented with 0.2% glucose with approximately 10^7 CFU/mL bacteria from fresh overnight cultures (also grown in M9 medium + 0.2% glucose) of the *P. aeruginosa* SMC4386-WT strain and the isogenic ΔCRISPR, ΔMADS and ΔCRISPRΔMADS strains. To these vials, 10^5 PFU/mL of phage DMS3*vir*-WT and either 10, 100 or 1000 PFU/mL of phage DMS3*vir*-methtylated were added, and incubated at 37°C while shaking at 180 rpm. In parallel, infection assays with 10^5 PFU/mL of phage DMS3*vir*-WT alone, and 10, 100 or 1000 PFU/mL of phage DMS3*vir*-methtylated alone were performed as control. The next day, phages were chloroform extracted and the titers were measured using spot assays onto lawns of *P. aeruginosa* SMC4386ΔCRISPRΔMADS strains. Plates were incubated overnight at 28°C.

Site directed mutagenesis

Catalytic mutant of *mad6* were generated through site directed mutagenesis as per manufacturer's guidelines. Briefly, a first step of PCR amplification of the plasmid pLola-*mad6*-MADSP was performed using primers mad6_HRD_Fw (5'-GCGGCTTGATgttGCA GTGGTGG-3') and mad6_HRD_Rv (5'- GCAATCTGTTGTGGACACAGAAG-3') (see Table S6), following a Kinase, Ligase and DpnI (KLD) treatment, as per the manufacturer's instructions. The primers were designed in order to mutate the HRD motif of *mad6* (D622N, based on eukaryotic mutations[66,67]), for the Aspartic Acid within this motif is the predicted catalytic residue functioning as a base acceptor for proton transfer.[68–70] The KLD mix was then transformed into chemically competent *E. coli* DH5α, following by plating onto selective (LBA with Gm) agar plates and incubated overnight at 37°C. The next day, 10 colonies were randomly selected for plasmid extraction using the Thermo Scientific GeneJET Plasmid Miniprep Kit (Thermo Scientific, USA) according to the manufacturer's instructions. The so extracted plasmids were sent for Sanger sequencing (Source BioScience, Cambridge, UK) using primers mad6_seq_For (5'- GTGGTGCGTGTGCTGGAT-3') and mad6_seq_Rev (5'-TCGTGTCCCACGGGTAGC-3') that produced an amplificon of 427 bp encompassing the region containing the desired mutation. Positive clones were then sent for Nanopore sequencing (Source BioScience, Cambridge, UK) to ensure correct amplification of the whole plasmid.

Mathematical modelling

Epidemiological dynamics (no phage evolution)

We develop a model to understand the dynamics of bacteriophages in a multiresistant bacteria population. Earlier studies have examined the evolution of Acr in well-mixed environments.[25,48] Here, we explore how the addition of a second resistance could affect the dynamics. In Figure S2D is showed a schematic representation of the phage life cycle (where we assume that bacteria are initially CRISPR resistant to the phage). The Acr-phage is able to infect resistant bacteria with a probability $1 - \rho$, where ρ is a measure of CRISPR efficiency. These infections can either lead in (i) the production of immunosuppressed cells with probability $r(1 - \phi)$, where r is is another measure of CRISPR efficiency and ϕ is a measure of anti-CRISPR efficiency, or (ii) they can result in cell lysis and the release of B virions with probability $(1 - r(1 - \phi))(1 - m)$, where m is a measure of MADS efficiency.

This yields the following system of ordinary differential equations (where $N = R + S$):

$$\begin{aligned}\frac{dR}{dt} &= \lambda R\left(1 - \frac{N}{K}\right) - aV(1-\rho)(1-(1-e)m(1-r(1-\phi)))R - dR + \gamma S \\ \frac{dS}{dt} &= a(1-\rho)r(1-\phi)RV - aV\,(1-(1-e)m)S - dS - \gamma S \\ \frac{dV}{dt} &= (aB((1-\rho)(1-(1-e)m)(1-r(1-\phi))R + (1-(1-e)m)S) - aN)V\end{aligned} \qquad \text{(Equation 1)}$$

The change in the total density of virus V at the beginning of an epidemic where $S = 0$ and $N = R$:

$$\frac{dV}{dt} = aN(B(1-\rho)(1-(1-e)m)(1-r(1-\phi)) - 1)V$$

In other words, the phage population can grow only when:

$$\phi > \phi_0 = \frac{1}{B(1-\rho)(1-(1-e)m)r} - \frac{1-r}{r}$$

Yet, if one introduces a large density of phages in the host population they will immunosuppress a fraction S/N of the cells. This will yield the following threshold

$$\phi > \phi_0 - \frac{S}{R}(B(1-(1-e)m) - 1)\left(\phi_0 + \left(\frac{1-r}{r}\right)\right)$$

In other words, we recover the results of Landsberger et al.[25] (in the case where $m = 0$) and extend it to the case where bacteria carry the MADS resistance. The above expression shows that increasing m always increases the threshold density of viruses above which the epidemic can take off (see Figure S2E).

Evolutionary dynamics of the phage (MADS escape)

In the following we consider an alternative model where the phage can acquire an epigenetic mutation allowing the virus to escape MADS (i.e., the parameter $e = 1$ for the escape mutant):

$$\begin{aligned}\frac{dR}{dt} &= rR\left(1 - \frac{N}{K}\right) - a(1-\rho)R((1-(1-e)m(1-r(1-\phi)))V + V^e) - dR + \gamma S \\ \frac{dS}{dt} &= a(1-\rho)r(1-\phi)R(V+V^e) - a\,((1-(1-e)m)V + V^e)S - (d+\gamma)S \\ \frac{dV}{dt} &= (aB(1-(1-e)m)((1-\rho)(1-r(1-\phi))R + S) - aN)V - \mu V \\ \frac{dV^e}{dt} &= (aB((1-\rho)(1-r(1-\phi))R + S) - aN)V^e + \mu V\end{aligned} \qquad \text{(Equation 2)}$$

We use this model to explore what happens if we allow some mutation to occur between V and V^e (i.e., $\mu = 0.0001$), showing that the tipping point for phage amplification shifts to higher initial phage densities as the strength of CRISPR immunity increases (see Figure S2F).

Another way to formalize the evolution of escape mutation (focusing on the frequency f^e of the mutant) where f^e is the frequency of the mutated virus:

$$f^e = \frac{V^e}{V^T}$$

with $V^T = V^e + V$ and:

$$\frac{dV^T}{dt} = (aB((1-\rho)(1-r(1-\phi))R + S)(1-(1-f^e)(1-e)m) - aN)V^T$$

In other words, the phage population V^T can only grow when:

$$\phi > \phi_0 = \frac{1}{B(1-\rho)(1-(1-f^e)(1-e)m)r} - \frac{1-r}{r}$$

Yet, if one introduces a large density of phages in the host population they will immunosuppress a fraction S/N of the cells. This will yield the following threshold

$$\phi > \phi_0 - \frac{S}{R}(B(1-(1-f^e)(1-e)m) - 1)\left(\phi_0 + \left(\frac{1-r}{r}\right)\right)$$

The change in mutant frequency is:

$$\frac{df^e}{dt} = \underbrace{f^e(1-f^e)}_{\substack{\text{genetic}\\ \text{variance}}} \underbrace{aB((1-\rho)(1-r(1-\phi))R+S)(1-e)m}_{\substack{\text{coefficient}\\ \text{of selection}}} \quad \text{(Equation 3)}$$

The Equation 3 captures what parameters govern the speed at which the mutant virus is expected to increase in frequency. In particular, higher m (stronger MADS), higher ϕ (stronger Acr), lower ρ or r (less effective CRISPR resistance, i.e., lower numbers of spacers in the CRISPR array) promote the evolution of the mutant virus. Besides, the parameter γ may also affect the strength of selection via its effect on the quantity of R cells. When γ is large, the immunosuppressed cells recover their immunity very fast, the density R increases which favors the increase in V^e frequency.

QUANTIFICATION AND STATYSTICAL ANALYSIS

All experiments were carried out in six biological replicates, except for the growth curves and complementation assays, which were carried out in four biological replicates, and for the efficiency of plaquing (EOP) assays, which were carried out in three biological replicates. Details of the statistical tests are provided in Table S2.